INVESTIGATING THE EFFECTS OF CORE LENGTH ON PORE VOLUME TO BREAKTHROUGH (PVBT) BEHAVIOR IN CARONATE CORE SAMPLES DURING MATRIX ACIDIZING WITH HYDROCHLORIC ACID

A Thesis

by

Mohamed Hashim Nour

Submitted to the Office of Graduate and Professional Studies of
Texas A&M University
in partial fulfillment of the requirements for the degree of

MASTER OF SCIENCE

Chair of Committee,	Hisham A. Nasr-El-Din
Committee Members,	Robert Lane
	Mahmoud El-Halwagi
Head of Department,	A. D. Hill

May 2014

Major Subject: Petroleum Engineering

ABSTRACT

Most literature contains Hydrochloric acid (HCl) carbonate acidizing experiments performed on short (2 - 6 inch) cores. These cores do not accurately represent reservoir conditions, as spent acid is not propagated for any appreciable distance along the length of the sample. In this work, HCl injection experiments are performed on both short (6 inch) and long (20 inch) calcite cores to investigate the pore volume to breakthrough (PVBT) behavior.

PVBT is defined as the volume of acid necessary to propagate the wormhole network from the inlet to the outlet of the core sample, divided by the pore volume of the core. HCl (5 and 15 percent by weight) injection core flood experiments were performed on 6 inch and 20 inch calcite (Indiana Limestone) cores. The cores were CAT scanned before and after acid injection to observe wormhole propagation. Core outlet effluent samples were collected and their calcium concentration was measured using Inductively-Coupled Plasma.

Results from core flood experiments show an increased PVBT for 20 inch cores compared to the 6 inch samples. Results from CAT scan experiments show enlarged worm-holing and face dissolution on the 20 inch cores compared to the 6 inch cores, due to increased acid spending at the same acid concentration, flow rate, and injection temperature. Results from experiments performed at various flowrates indicate the existence of an optimum injection rate for 20 inch cores, just as in 6 inch cores. This study summarizes and explains the results obtained from the aforementioned experiments.

DEDICATION

I dedicate this thesis to my parents and sisters.

ACKNOWLEDGEMENTS

I would like to thank my Academic Adviser, Dr. Hisham Nasr-El-Din, for his guidance and support throughout the course of this research. I would also like to thank my thesis committee members, Dr. El-Halwagi and Dr. Lane, for their support.

I would also like to thank all my friends and colleagues in the petroleum engineering department and in the other departments at TAMU for their valuable guidance, support, and good company

Finally, I would like to issue a heartfelt thanks to my family for their endless love and support, without which this work would have been impossible.

TABLE OF CONTENTS

Page

LIST OF FIGURES

Page

LIST OF TABLES

Page

CHAPTER I

INTRODUCTION

BACKGROUND

Matrix Acidizing is the oldest stimulation technique for carbonate formations. Such treatments have been performed on carbonate formations for many decades (Williams, B., Gidley, J., and Schechter, R.S. 1979). Matrix acidizing is the preferred stimulation technique for medium to high permeability carbonate formations (50 md or more) (Robert, J.A., and Crowe, C.W. 2000). However for tight carbonate formations (less than 10 md), acid fracturing produces the best stimulation results via long acid-etched fractures (Hill et al. and Bazin et al. 1995). In addition, matrix acidizing is the stimulation technique of choice for bypassing drilling, work-over, or completions induced formation damage in limestone reservoirs.

Hydrochloric acid (HCl) has been the most popular stimulation fluid for these treatments, due to factors such as its high reaction rate, low cost, and tendency to form soluble reaction products (Fredd, C.N. and Fogler, H.S. 1998a and Buijse et al. 2004). The injection of HCl into carbonate formations dissolves the matrix and causes the formation of channels called wormholes. These wormholes act as highways that can carry formation fluids to the wellbore and enhance production (Nierode and Williams 1971). Another advantage associated with the induced wormholes is that they can be used to bypass formation damage in the near wellbore region. For acid treatments to be successful in the field, numerous factors must be taken into account. Two of the most important factors that are imperative to the success of an acid treatment are additives and

acid placement. Additives are necessary to protect equipment from corrosion, ensure correct formation wettability, and reduce drag and frictional forces. These are just some of the main uses for acidizing additives, and a plethora of chemicals exist that are added to acid formulations to perform various specific tasks. Acid placement also plays an important role in the success of acid treatments. Failure to properly place acid in the target zone is a leading cause of failed acidizing jobs. These are some of the main factors that could affect wormhole propagation, and a great amount of specialized literature can be referred to for a more detailed discussion of their effects.

The propagation of acid-induced wormholes in carbonate samples is a function of multiple factors. Some of the main factors as stated by Hoefner and Fogler (1987, 1988, and 1989) are rock composition, pore structure (uniformity vs. large scale heterogeneities), and temperature. The importance of factors such as rock composition and pore structure is understood by realizing that wormholes are essentially a highly ramified set of flow channels that are orders of magnitude greater in diameter than the existing pores in the matrix. However this can be untrue for formations or samples that contain large scale heterogeneities. Temperature is an important factor as it affects the reaction rate of HCl with calcium carbonate, with the trend being an increased reaction rate with increasing temperature. The flow rate of acid injected into the rock to induce dissolution and wormholing will also play a factor in the geometry of the resulting wormholes (Talbot and Gdanski 2008). This is because the dissolution process occurs via a heterogeneous reaction, and the acid injection rate affects the mass transfer of acid

to the surface of the rock, and of the products away from the surface and back into the bulk.

Most acidizing literature that tackles the issue of wormhole propagation from an experimental angle uses tests performed on short (2 - 6 inch) core samples. These small samples do not accurately represent reservoir conditions, because spent acid is not propagated for any appreciable distance along the length sample. In this work, HCl injection experiments are performed on both short (6 inch) and long (20 inch) calcite samples to investigate the pore volume to breakthrough (PVBT) behavior.

LITERATURE REVIEW

Matrix acidizing in carbonate formations is a heterogeneous chemical reaction occurring in a porous medium; and involves the transport of reactants to the rock surface, the reaction at the surface, and transport of the products back to bulk (Daccord 1987). Fredd and Fogler (1999) state that this process is accompanied by a continuous alteration of the pore structure of the rock matrix. Wormholes, which is the name given to the highly conductive channels formed by this heterogeneous reaction, are capable of bypassing damaged zones around the wellbore, so that the reservoir fluids can be produced with more efficiency. The structure of the formed wormholes is an important factor when evaluating the outcome of an acidizing treatment.

Various models have been developed by many researchers in an attempt to better understand and quantify the wormholing process. Schechter and Gidley (1969) treated the pores as randomly distributed cylindrical tubes and evaluated a mechanism for pore enlargement. They also looked at how the surface reaction causes changes in pore

distribution, and an equation was developed to describe pore structure evolution. They concluded that the pores are enlarged by reaction and that collisions can cause two pores to become one larger pore. These larger pores, formed by the enlargement of smaller pores, determine the response of the system to acid injection.

Daccord et al. (1989) developed a wormhole propagation model. This model was based on the dissolution pattern created by injecting water into a rectangular block of plaster. The model aimed to quantify wormholes by a unique parameter, defined as the equivalent hydraulic length. This model was based on the diffusion limited mechanism for acid transport to the rock surface. However, it did not take into account the fluid loss process, which is an important factor in wormhole growth. Since this model was based on a dissolution pattern derived from injecting water into a block of plaster, it may not accurately emulate the dissolution pattern observed in carbonate acidizing. Hence the model created by Daccord should be treated with caution when applied to carbonate acidizing.

Daccord et al. (1993 a & b) also concluded that for such highly reactive systems, an optimum injection flow rate exists. This optimum injection flow rate is now an ubiquitous concept and has become the basis for subsequent wormhole propagation studies. The work done by Daccord focused on identifying the optimum conditions for carbonate acidizing in addition to studying the wormhole propagation mechanism.

Multiple experimental-based carbonate acidizing studies concluded that an optimum injection rate exists for carbonate acidizing. Wang et al. (1993) performed a series of carbonate acidizing experiments and concluded that the optimum injection rate

does exist. This is an injection flowrate that leads to the minimum amount of acid being required to propagate the wormhole network from the inlet to the outlet of the core sample (Frick et al. 1994).

This optimum injection rate is a critical parameter in acidizing, and has become the focus of many subsequent carbonate matrix acidizing models. A theory was developed by Huang et al. (1997) to predict the optimum injection rate. This theory was tested with a series of laboratory experiments. Their model was based on a cylindrical flow system, and it was developed to represent the flow field associated with a wormhole propagating from the wellbore. This allows for predicting field parameters from laboratory data.

RESEARCH OBJECTIVES

In matrix acidizing, PVBT is defined as the volume of acid necessary to propagate the generated wormhole network from the inlet to the outlet of the sample, divided by the pore volume of the sample. This quantity is important for designing acid treatments, and it appears in many popular wormhole propagation models (Volumetric Model, Buijse-Glasbergen Model, Furui et al. Model) and in expressions to predict skin evolution. The objectives of this experimental study are as follows:

1) To investigate the effects of acid spending and propagation of spent acid on PVBT behavior (by varying core sample length) when injecting HCl (5 and 15 percent by weight) in core flood experiments performed on 6 inch and 20 inch calcite (Indiana limestone) cores

2) To investigate the effects of acid injection flowrate in 20 inch cores on PVBT behavior when injecting HCl (15 percent by weight) at various flow rates (5, 10, and 20 cm^3/min) in core flood experiments performed on 20 inch calcite (Indiana limestone) cores
3) To study the effect of CO_2 generated as a reaction product, via performing coreflood acid injection tests at 1000 psi and 1850 psi backpressures
4) To investigate the formation damage resulting from the injection of supercritical CO_2 into brine saturated calcite cores, via the deposition of $CaCO_3$

CHAPTER II

MATERIALS AND METHODS

Chapter II is divided into two parts. In the first part, titled "Materials", the laboratory apparatus that was employed in the experimental study is described. The chemicals used to prepare solutions employed in the experiments are also described in the "Materials" section. In the second section, titled "Experimental Methods", the preparation of chemical solutions and core samples for acid injection and supercritical CO_2 injection tests is described.

MATERIALS

Coreflood Apparatus

The coreflood setup was used to emulate matrix stimulation treatments. A back pressure of 1000 or 1850 psi (depending on the specific test) was applied to keep the CO_2, generated as a reaction product, in solution. A pressure transducer was connected to a computer to monitor the pressure drop across the core during the experiments. The transducer employed is an IDP-10 model manufactured by Foxboro Invensys, and its accuracy is 0.001% of the calibrated range of the transducer. Two different transducers were used to monitor the pressure drop, depending on which setup was used for each test. Their calibrated range is 1000 and 300 psi respectively. A Teledyne ISCO D-series D1000 precision syringe pump, that had a maximum allowable working pressure of 2000 psi, was used to inject fluids into the core sample. All the coreflood tests were run at a temperature 150 °F using 6 and 20 inch Indiana limestone core samples and 5 or 15 wt% HCl solution, depending on the specific test. In order to maintain the acidizing process at

a constant temperature, two temperature controllers were used. The temperature of the preheated fluids coming from the accumulators was controlled by a compact bench top CSC32 series, which has a 4-digit display, a 0.1° resolution, uses a type K thermocouple and two outputs (5 A 120 Vac SSR), and has an accuracy of ±0.25% full scale ±1°C. Using LabView® software, the pressure drop across the core sample was monitored at all times during treatment. The LabView® data acquisition software was set up so as to collect a reading of the pressure difference between the core sample inlet and outlet once every five seconds. This data collection scheme was employed when measuring the permeability of Indiana limestone core samples before acid injection experiments and also during both acid injection and supercritical CO_2 injection experiments. A diagram of the coreflood apparatus is shown in Figure 2.1.

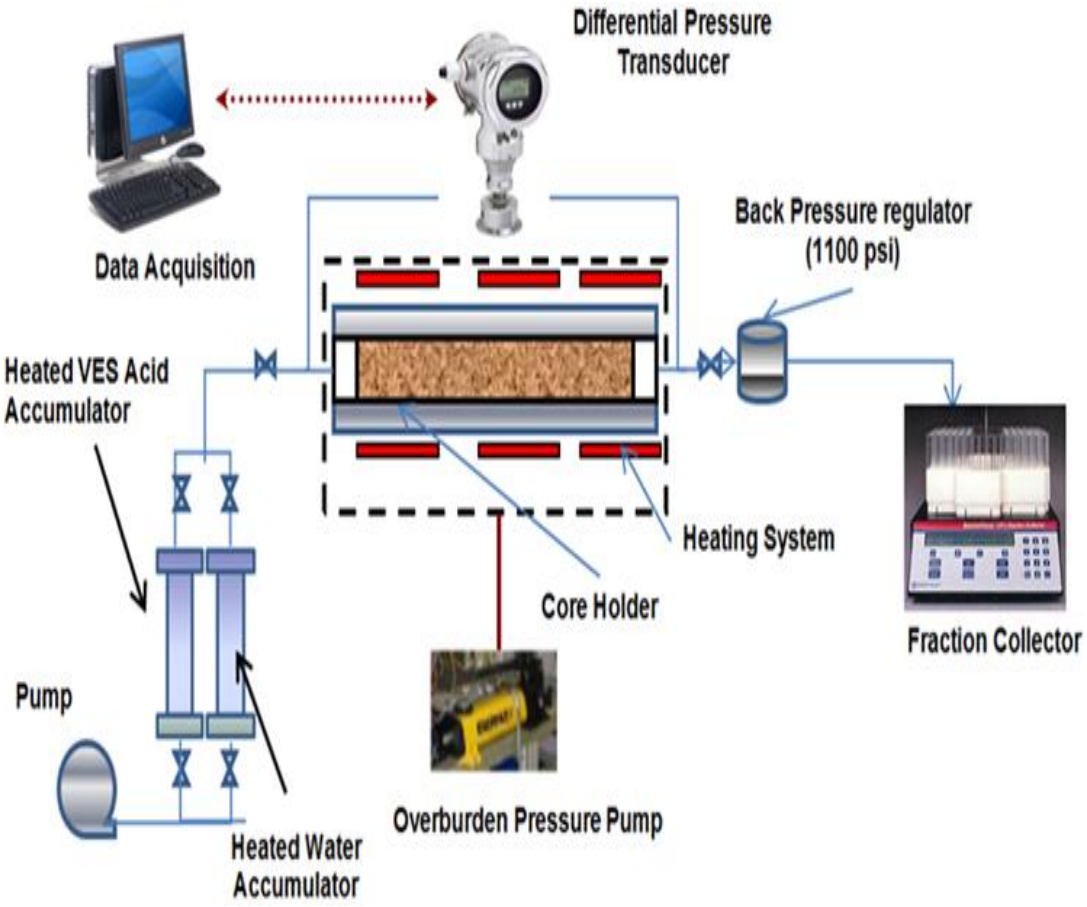

Figure II.1: Coreflood apparatus schematic

Inductively Coupled Plasma (ICP) Analysis Apparatus

Inductively Coupled Plasma (ICP) atomic spectroscopy was used to measure the concentration of calcium cations (Ca^{2+}) present in the effluent collected from acid injection and supercritical CO_2 injection experiments. This is an analytical technique where the ions in question absorb energy (provided by a plasma torch) and thus are promoted from the stable, ground state to an excited, high-energy state. The ions then decay back to the ground state, and release energy of a specific wavelength. Every

element possesses its own specific set of energy levels, and subsequently its own set of absorption and emission wavelengths.

The ICP equipment employed in this experimental study was an Optima 2011 Series DV instrument manufactured by Perkin Elmers. This device employed an optical emission spectrometry (OES) technique for the detection of the amount of calcium ions present in solutions. In this technique, the sample was subjected to high temperatures that caused a high amount of collisional excitation in the calcium ions. The ions then decayed to ground state through thermal and radiative energy transitions. The intensity of the light emitted at specific wavelengths was measured and used to determine the concentrations of calcium ions in solution.

Figure 2.2, displayed below, contains an illustration of the ICP device that was employed in this study.

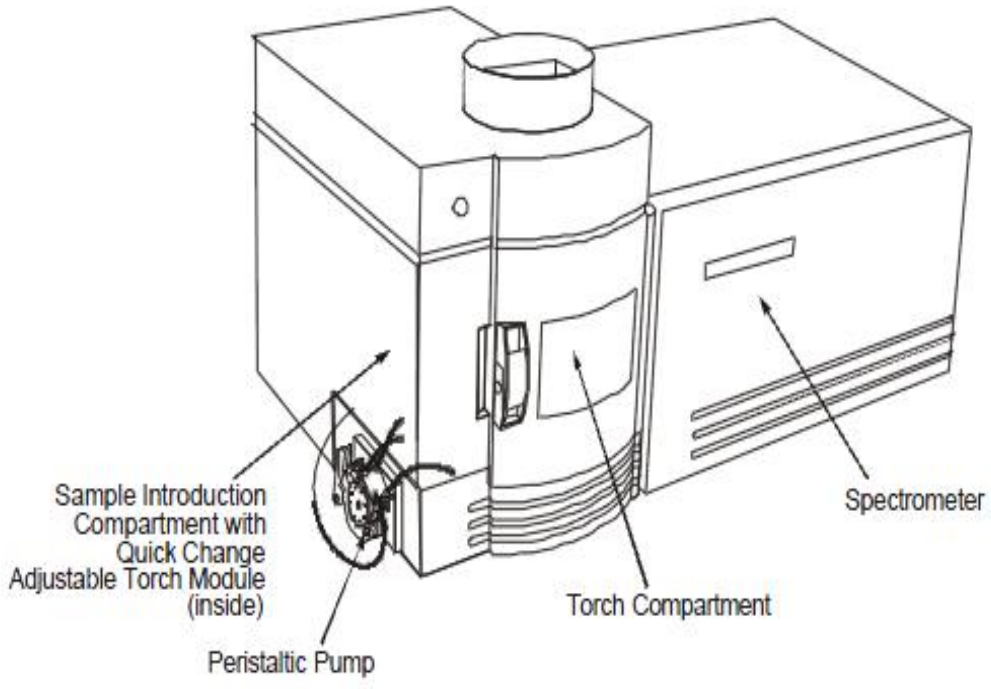

Figure II.2: ICP analysis apparatus

CAT Scanner

Computer Tomography (CT) scans were used to analyze core samples before and after acid and supercritical CO_2 injection experiments. The scans were performed before the tests to ensure that no large scale heterogeneities that could affect experimental results were present in the core samples. These heterogeneities could be compositional or structural. The main compositional heterogeneities that were to be avoided for the purpose of this work were the presence of dolomite or anhydrite streaks, which would react differently than calcite with HCl and affect the generation and propagation of wormholes. Structural heterogeneities include vugs and long fractures which would have allowed the acid to bypass the process of pore enlargement through reaction. For acid

injection tests, scans were performed after the experiments to observe and analyze the wormhole network generated by acid-induced dissolution of the matrix.

A Universal HD-350 computed tomography system was employed in the experimental study. This apparatus featured a versatile gantry system, and was powered by a 140kV power source. It featured a high-throughput capability, with scans speeds up to one second. The system was capable of taking image slices that were 1, 2, 3, 4, 5, 8, and 10mm in diameter. A photograph of the system, provided by the manufacturer, is displayed in Figure 2.3.

Figure II.3: CAT scan apparatus

Auto-titration Apparatus

Titration with NaOH solution of a known molarity was performed on effluent samples collected from coreflood acid injection tests. This procedure was conducted to determine the live acid content present in effluent samples. This in turn enabled the determination of the breakdown of acid that travelled through the generated wormhole network, in terms of reacted and unreacted acid.

An auto-titration apparatus was employed to determine the live acid content of samples in question. The equipment employed in this study was an Orion 950 analytical titrator, manufactured by Thermo Scientific. This equipment was used to provide fast and accurate automatic potentiometric titrations. The calibration, measurement, and verification of the results were performed automatically by the machine, and required the use of pre-set standard pH solutions. A photograph of the apparatus, provided by the manufacturer, is displayed in Figure 2.4.

Figure II.4: Auto-titration apparatus

Capillary Viscometer

An Ubbelohde type capillary viscometer (also known as a suspended-level viscometer) was used to determine the viscosity of brine solutions used in supercritical CO_2 injection experiments. The time taken for the sample solution to travel between two calibrated marks was measured in seconds. That time was then multiplied by the apparatus constant provided by the manufacturer to determine the kinematic viscosity of the solution. Using the density of the brine solution, the dynamic viscosity was then determined. A photograph of the apparatus, provided by the manufacturer, is displayed in Figure 2.5:

Figure II.5: Ubbeholde capillary viscometer

Hydrochloric Acid (HCL)

The HCL used for all acid injection experiments was purchased at a weight concentration of 36.5%. The acid was then diluted to the required weight concentration (5 or 15 wt.%) using de-ionized water.

Corrosion Inhibitor

The addition of a corrosion inhibitor is important to protect the experimental setup. A corrosion inhibitor labeled is called A270 was used, and it was provided by Schlumberger. The full list of components of this inhibitor and their amounts were proprietary, however an MSDS was provided.

Carbon Dioxide

The carbon Dioxide was provided by the supplier (Cuevas) in gas tanks at a pressure of 600 psi. The carbon dioxide is of high purity, and according to the supplier it is 99.8% pure.

Carbonate Core Samples

For all acid injection and supercritical CO_2 injection experiments, the core samples used were Indiana limestone cores provided by Kocurek Industries. The cores originally came in the form of cuboid blocks, and cylindrical samples (6 and 20 inch) were drilled form these blocks. The blocks were labeled with estimated permeability ranges by the supplier. The samples elected for this work were from blocks estimated to be of 50mD permeability, even though the permeability of the actual core samples drilled out of these blocks varied.

Sodium Chloride

Laboratory research-grade sodium chloride (NaCl) crystals were used to prepare brine solutions that would then be used to saturate cores for supercritical CO_2 injection experiments.

EXPERIMENTAL METHODS

Acid Preparation

The HCl acid solution was diluted from 36.5 wt% to 5 or 15 wt%, depending on the specific test. A270 corrosion inhibitor was added to protect the experimental equipment, and its concentration was 0.4% of the acid solution on a volume basis. The acid was mixed using a magnetic stir plate and a magnetic stir bar.

Brine Preparation

Sodium chloride solution used for supercritical CO_2 injection tests was prepared in a plastic beaker using an automatic electric-motor driven mixer. The solution was prepared to yield either a 6 or 12% sodium chloride solution, on a weight basis, depending on the specific test to be performed. The brine solution was prepared using de-ionized water.

Supercritical CO_2 Preparation

The CO_2 provided by the manufacturer was in the tank at a pressure of 600 psi. To pressurize the CO_2 and make it supercritical, the gas was first made to completely fill an empty one-liter accumulator at 600 psi. The accumulator was then sealed and a syringe pump was used to decrease the volume of the accumulator, hence increasing the pressure. When the pump pressure was at a value of 1400 psi, the pump was stopped and the accumulator was now ready to inject supercritical CO_2 (at a pressure of 1400 psi).

Core Sample Preparation

The Indiana limestone core samples (6 and 20 inch) were first drilled out using an electromechanical rotating drill and a stainless-steel, diamond-tipped drill bit. The core samples were first completely dried. This was achieved by heating the samples in an oven at 300 °F for five hours. After drying, the weight of the cores was recorded. The cores were then saturated with de-ionized water in a chamber under vacuum. They were left for 6 hours in the de-ionized water-filled vacuum chambers to ensure saturation of the pore space. By weighing the core samples after saturation and comparing that number to the dry weight, the amount of water required to completely fill the pore space

could be determined. The density of the de-ionized water was then used to obtain the pore volume and porosity of the core samples from the weight of de-ionized water occupying the pore space.

The next step in core sample preparation was to measure the permeability of each core sample. This was done using the coreflood apparatus, the mechanical details of the apparatus were discussed in detail in the previous section. To measure the permeability of a core sample, de-ionized water of a known viscosity was injected into the de-ionized water-saturated core sample. This was done at three different flow rates (1, 3, and 5 cm^3/min) and the stabilized difference in pressure between the core sample inlet and outlet was measured and recorded. Using the measured pressure difference, the viscosity and flow rate of de-ionized water, and the cross-sectional area and length of the core sample, the permeability was calculated using the form of Darcy's law derived for linear, incompressible flow. Since the pressure drop was measured at three different flow rates, the permeability was also calculated three different times, and an average was used (the three permeability values obtained for each core sample were always in close agreement). The core samples were then analyzed via a CT scanner, to ensure that there were no heterogeneities that could affect the acid injection or supercritical CO2 injection tests.

CHAPTER III

INVESTIGATING THE EFFECTS OF CORE LENGTH ON PVBT

Chapter III is divided into two parts. In the first part, titled "Experimental Plan", the laboratory tests performed to evaluate the effect of core length on PVBT are outlined. The experimental procedure that is employed in these tests is also described. In the second part, titled "Results and Discussion", the results of each experiment are presented and the immediate significance of the findings is discussed. A more detailed treatment of the results and more comparative analysis are included in Chapter VI.

EXPERIMENTAL PLAN

The following experiments, tabulated in Table 3.1, were performed to evaluate the effects of core length on PVBT in Indiana limestone cores. All experiments were performed at an acid (HCl solution) injection flowrate of 5 cm^{3}/min and a temperature of 150 °F.

Table III.1: Experimental Outline for Chapter III

Experiment Number	Core Name	Core Length (inch)	HCl Concentration (wt. %)	Backpressure (psi)
1	B1-1	6	5	1000
2	B1-5	20	5	1000
3	B1-6	20	15	1000
4	B1-9	20	5	1850

The procedure employed to prepare the core samples for acid injection was outlined in Chapter II, in the section titled “Core Sample Preparation”. The process involved saturating the cores with DI water to determine the porosity and pore volume of each sample, and then running DI water through the saturated core samples at different flowrates to determine their permeability. The cores were then CT scanned to check for heterogeneities and ensure that they are suitable for acid injection.

After the aforementioned process is completed, the cores were then ready for acid injection. The acid injection process was initiated by first turning on the heater then setting the temperature controller to the desired temperature, which was 150 °F for all experiments. DI water was then allowed to run and the temperature, flowrate, and pressure drop across the core were allowed to stabilize. After that, injection was switched from DI water to HCl solution at 5 cm3/min. Acid injection continued until breakthrough was reached, which was observed via both visual inspection and a sharp decrease in the pressure drop across the core sample. When determining the volume of acid necessary to cause breakthrough, the dead-volume associated with apparatus was subtracted to eliminate that source of experimental error. The corrected volume could then be divided by the pore volume of the core sample to obtain a pore volume to breakthrough (PVBT) value.

After breakthrough, injection was switched to DI water. Two to three pore volumes of DI water were injected to flush the core sample and the apparatus clean of HCl. Effluent samples were collected during both HCl injection and the subsequent DI

water flush, and calcium ion concentration in the effluent samples was measured using ICP.

The treated cores where then CT scanned to study the geometry of the wormhole network generated by acid-induced dissolution. The density of the effluent samples was measured, and the samples were titrated with NaOH solution of a known molarity to determine the weight percentage of live acid in the samples. Finally, the porosity of the core samples post acid-injection was then determined.

RESULTS AND DISCUSSION

The results for Experiment 1 are displayed in Table 3.2.

Experiment 1: 6 inch Indiana limestone core with 5 wt.% HCl

Table III.2: Summary of Results for Experiment 1

Core Name	B1-1
Pre-acidizing Porosity (%)	12.76
Pre-acidizing Pore Volume (cm3)	22.17
Pre-acidizing Permeability (md)	172.9
Post-acidizing Porosity (%)	16.2
Dissolved Matrix (g)	5.93
Pore Volume to Breakthrough	1.2

Figures 3.1 and 3.2 are photographs of the core sample's inlet and outlet after acid injection:

Figure III.1: B1-1 inlet after acid injection

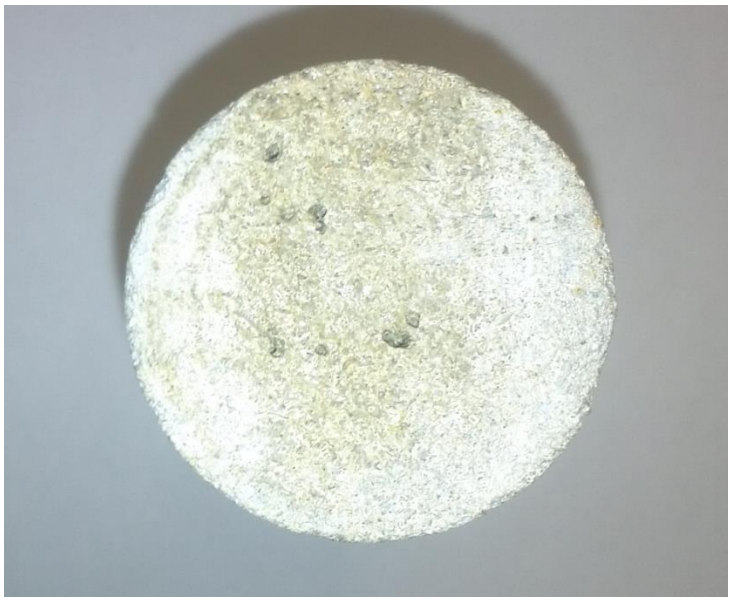

Figure III.2: B1-1 outlet after acid injection

The acid-induced wormholing can be observed in the core inlet and outlet displayed above. Figures 3.3 and 3.4 show CT scans of the core sample before and after acid injection:

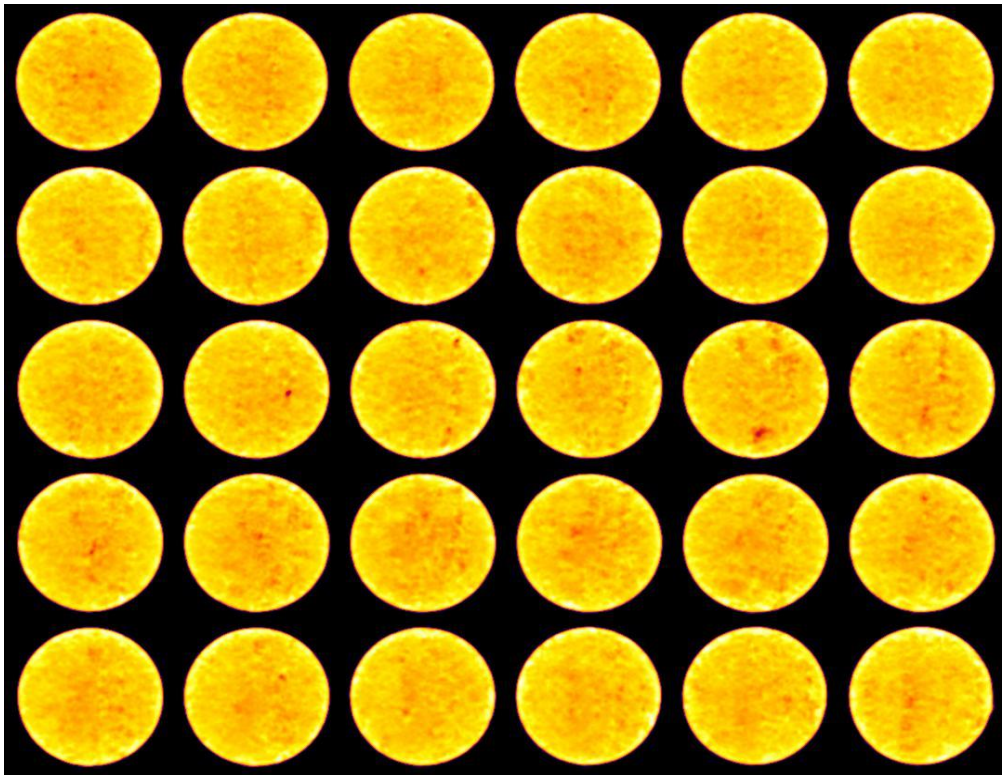

Figure III.3: CAT scan of B1-1 before acid injection

The figure above indicates the presence of some vugs in the core sample (red patches), correlating with its high permeability. The lithology of the core sample appears to be homogenous; there are no major solid white patches or streaks appearing in the bulk of the core sample. Such patches indicate the presence of a denser lithology, such as dolomite or anhydrite.

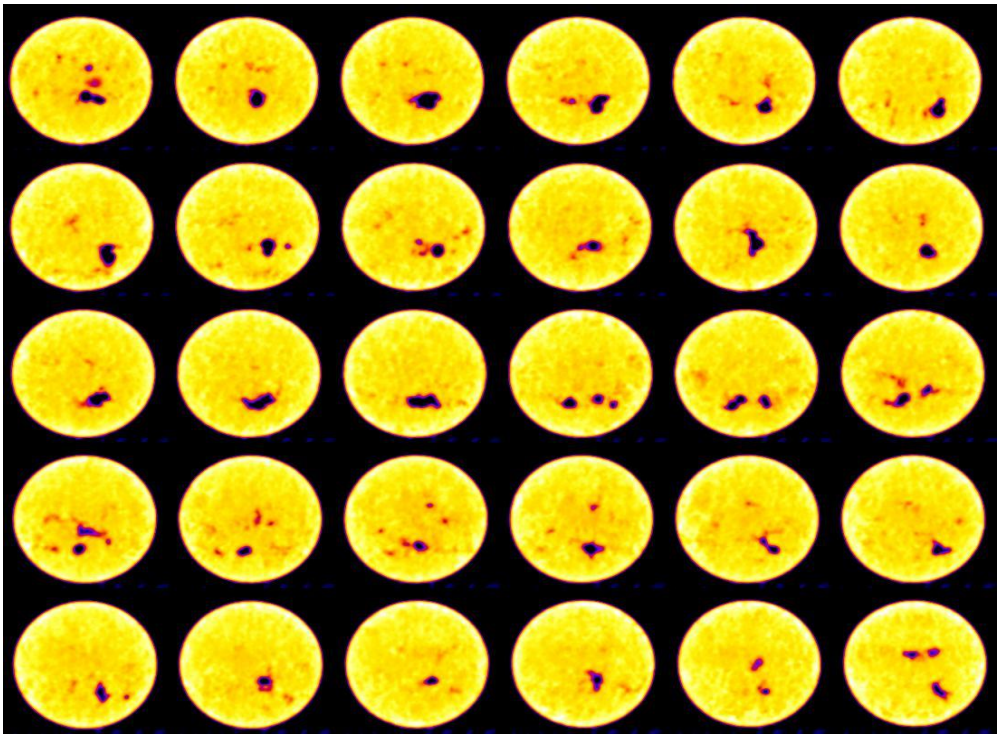

Figure III.4: CAT scan of B1-1 after acid injection

The propagation of the acid-induced wormhole network can be observed in Figure 3.4. Figure 3.5 displays the pressure drop across the core sample during the acid injection procedure:

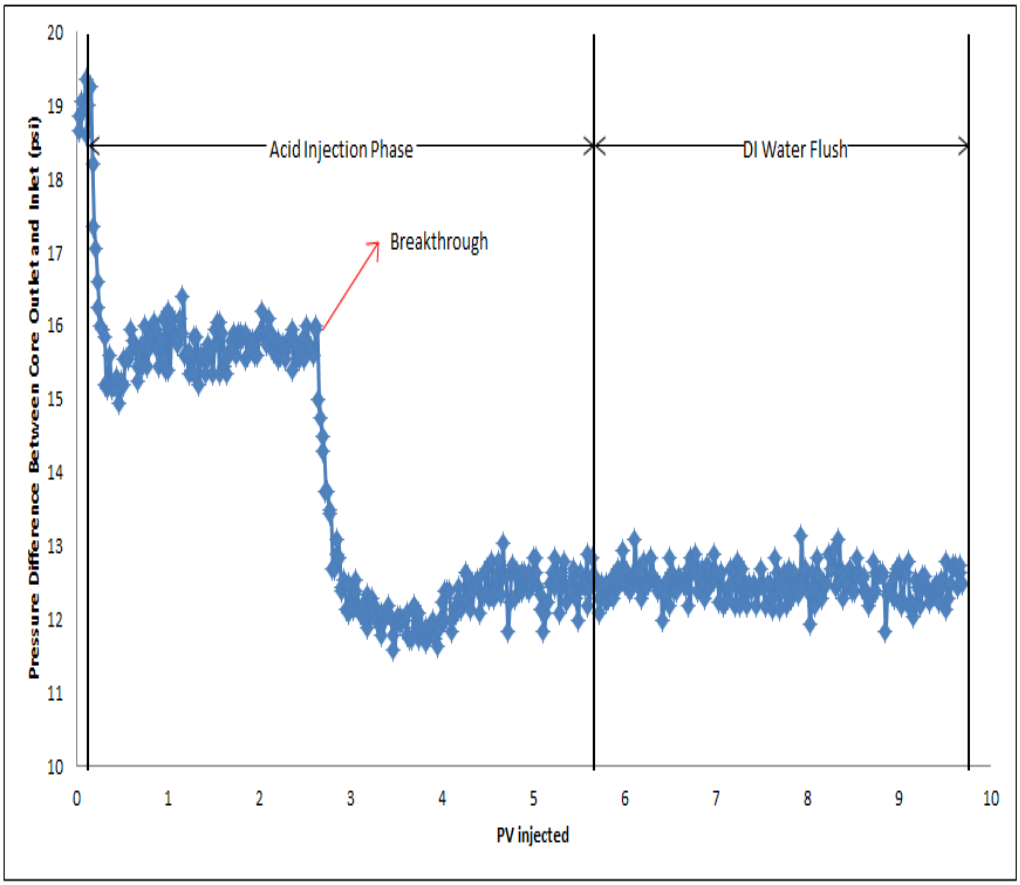

Figure III.5: Pressure drop across the core sample for Experiment 1

As the figure above indicates, acid injection starts at a PV of 0.225. There is an initial pressure drop immediately after injection is switched to acid. This is due to the quick start of the wormholing process, owing to the aggressive attack by the highly reactive HCl. The PVBT value for this test is 1.2.

The live acid concentration in the collected effluent samples was determined via titration. Figure 3.6 displays the live acid concentration versus pore volumes injected.

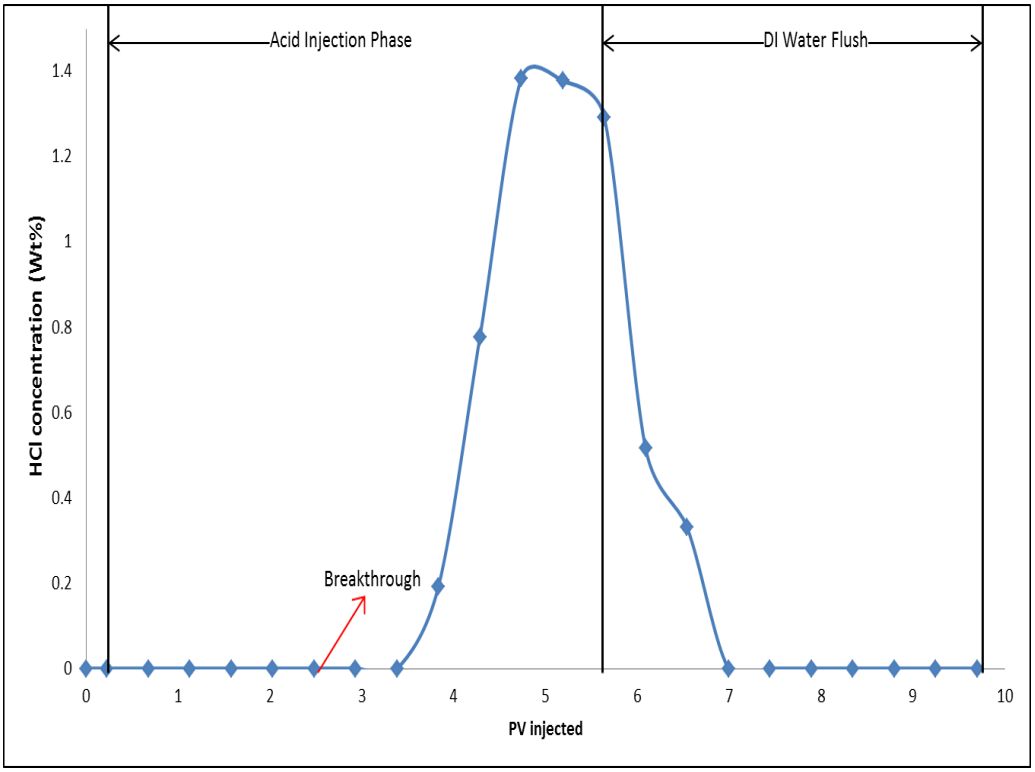

Figure III.6: Live acid in core effluent for Experiment 1

As the figure above indicates, HCl concentration begins to rise at a value of cumulative PV injected equal to 3.38. HCl concentration reaches its maximum value of 1.38 percent by weight at a cumulative PV injected equal to 4.73. Figure 3.7 below displays the concentration of calcium ions versus the cumulative pore volumes injected.

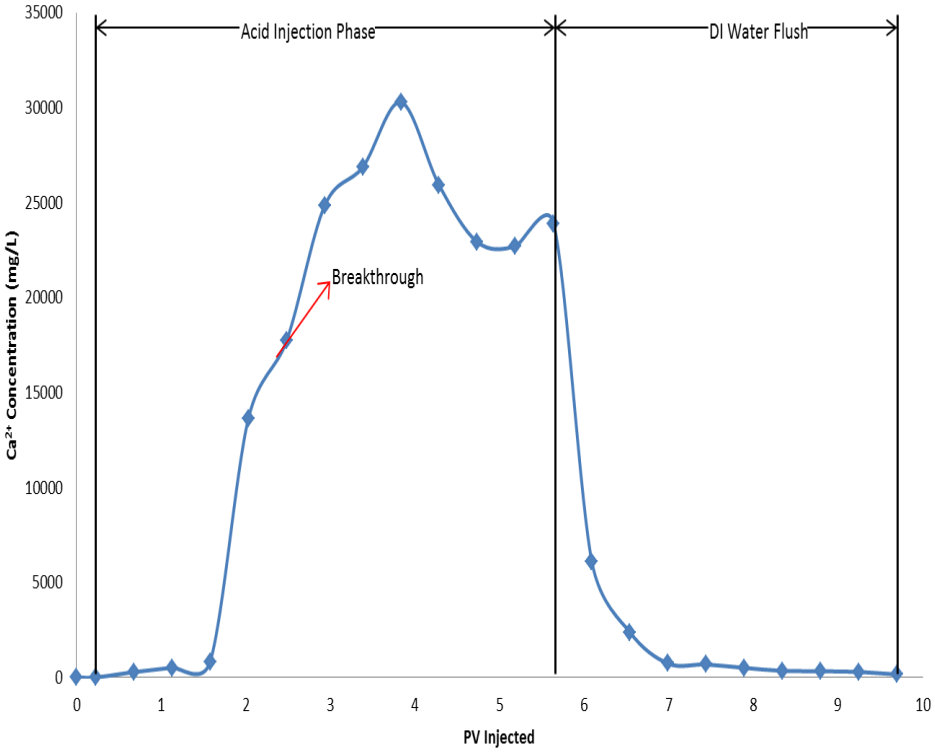

Figure III.7: Calcium ion concentration in acid injection effluent for Experiment 1

Calcium ion concentration starts increasing after 1.355 pore volumes of acid were injected. The concentration continues to rise after the breakthrough point of 2.304 PV. Calcium ion concentration reaches a maximum at 3.605 PV of acid injected, then drops sharply when the DI water flush is started at 5.64 PV. The results for Experiment 2 are displayed in Table 3.3.

Experiment 2: 20 inch Indiana limestone core with 5 wt.% HCl

Table III.3: Summary of Results for Experiment 2

Core Name	B1-5
Pre-acidizing Porosity (%)	14.27
Pre-acidizing Pore Volume (cm3)	82.67
Pre-acidizing Permeability (md)	14
Post-acidizing Porosity (%)	21.01
Dissolved Matrix (g)	38.8
Pore Volume to Breakthrough	6.53

Figures 3.8, 3.9, 3.10, and 3.11 are photographs of the core sample's inlet and outlet, before and after acid injection respectively.

Figure III.8: B1-5 inlet before acid injection

Figure III.9: B1-5 outlet before acid injection

Figure III.10: B1-5 inlet after acid injection

Figure III.11: B1-5 outlet after acid injection

After acid injection, some dissolution of matrix at the outside surface of the core was observed. This dissolution marks points where the acid broke through prematurely but was forced to continue lengthwise along the core axis by the rubber sleeve surrounding the core. This is displayed in the Figures 3.12 and 3.13.

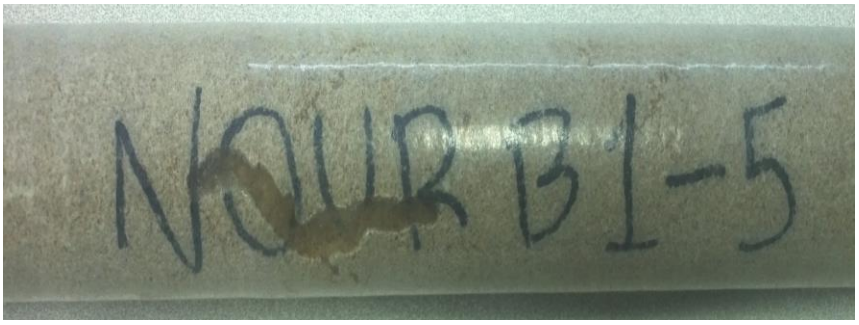

Figure III.12: B1-5, displayed lengthwise, after acid injection

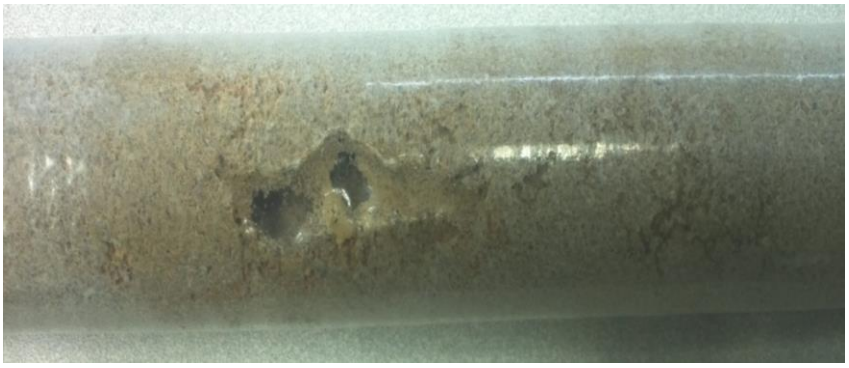

Figure III.13: Surface dissolution on B1-5 after acid injection

Face dissolution can be observed at the inlet, in addition to a large wormhole size. This implies that for 5 wt% HCl injected at 5 cm^3/min, once the wormholing has begun the flow rate is slow enough to cause face dissolution and enlarge the formed wormhole. The wormhole can be observed at the outlet where the acid broke through.

Figures 3.14 and 3.15 show CT scans of the core sample before and after acid injection respectively.

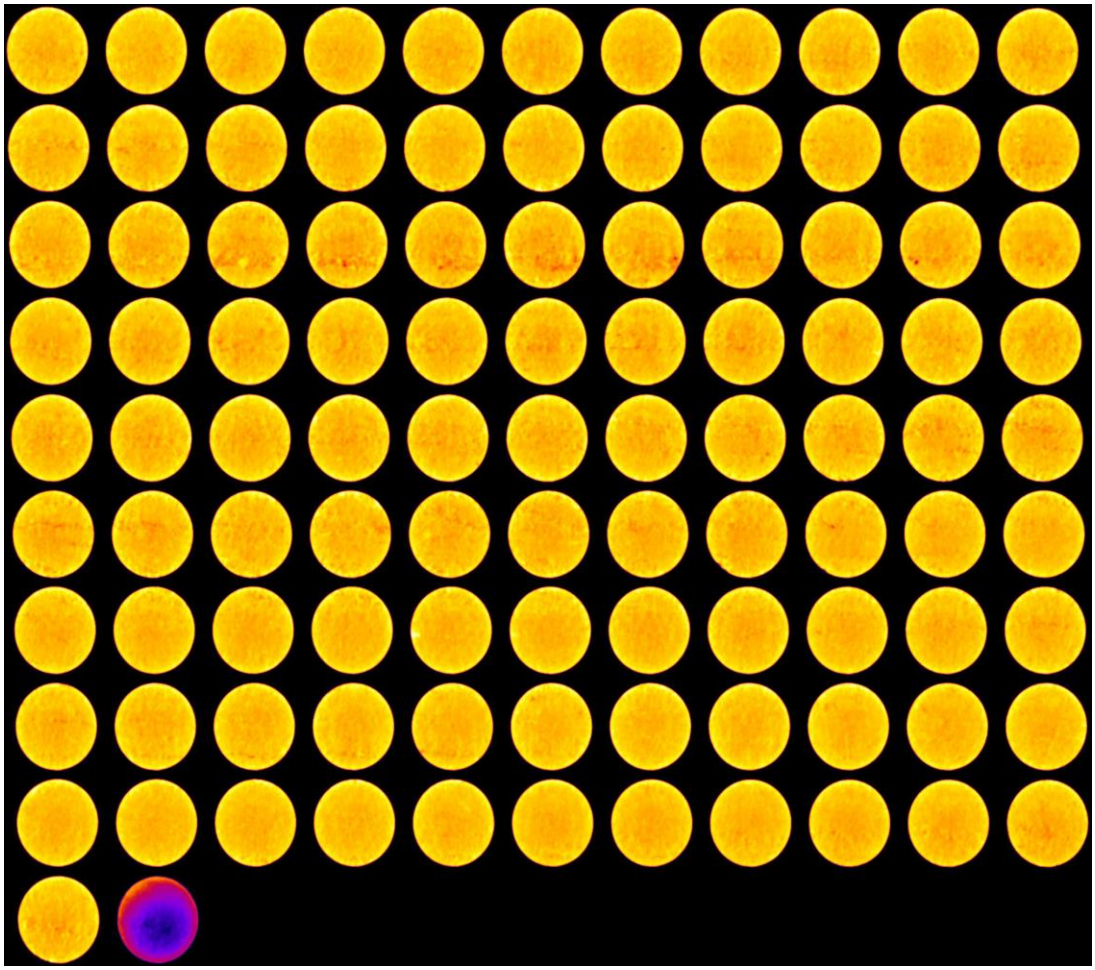

Figure III.14: CAT scan of B1-5 before acid injection

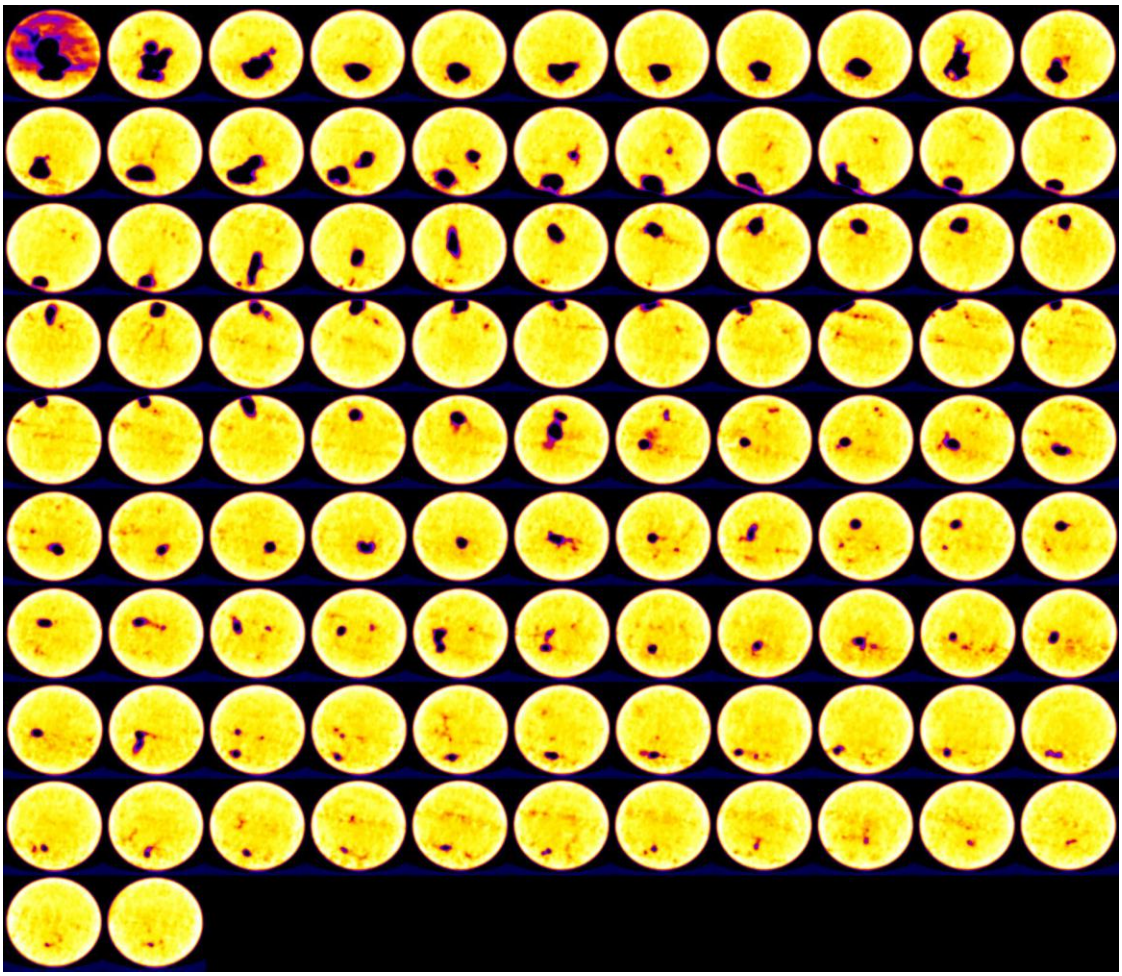

Figure III.15: CAT scan of B1-5 after acid injection

The propagation of the acid-induced wormholes can be observed in the previous figure. The wormholes closer to the inlet are much larger than those closer to the outlet. As the acid propagates deeper into the core, it spends as it reacts with the walls of the wormholes. Also, there is less live acid reaching the tip of the wormhole deeper into the core compared to the inlet. Therefore the acid attack becomes progressively less aggressive and the size of the wormhole becomes progressively smaller. Figure 3.16 displays the pressure drop across the core sample during the acid injection procedure.

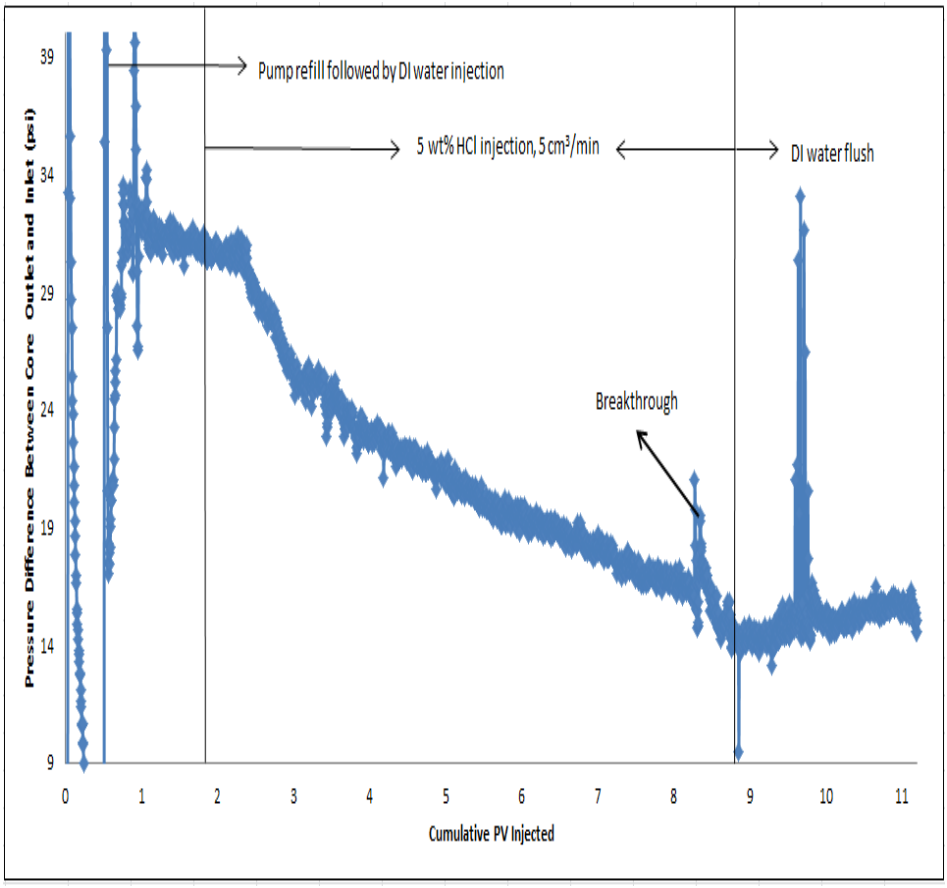

Figure III.16: Pressure drop across core sample for Experiment 2

The pressure difference continues to decrease after acid injection due to wormhole formation as the acid dissolves the matrix. Acid injection ends and DI water flush starts at PV of 8.8. The breakthrough occurs after 6.53 pore volumes of acid were injected. The live acid concentration in the collected effluent samples was determined via titration. Figure 3.17 displays the live acid concentration versus pore volumes injected.

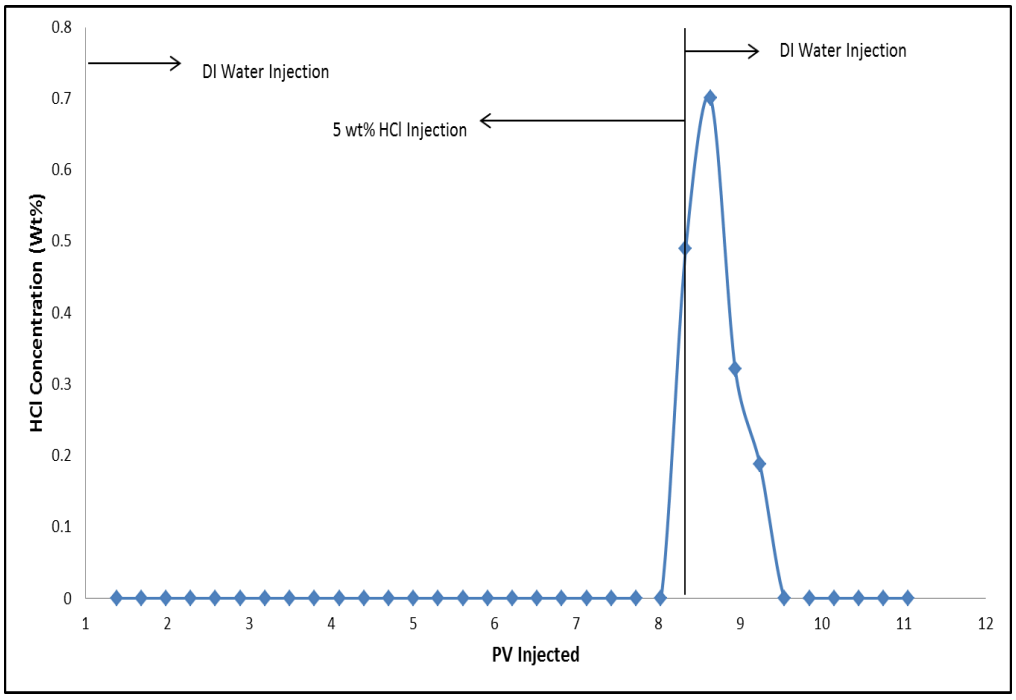

Figure III.17: Live acid concentration in acid injection effluent for Experiment 2

HCl concentration in the effluent samples is zero until the breakthrough point where it rises sharply. HCl concentration in the effluent reaches its maximum value of 0.7 wt% after the breakthrough and then declines sharply as DI water is immediately injected. Figure 3.18 displays the concentration of calcium ions versus the cumulative pore volumes injected.

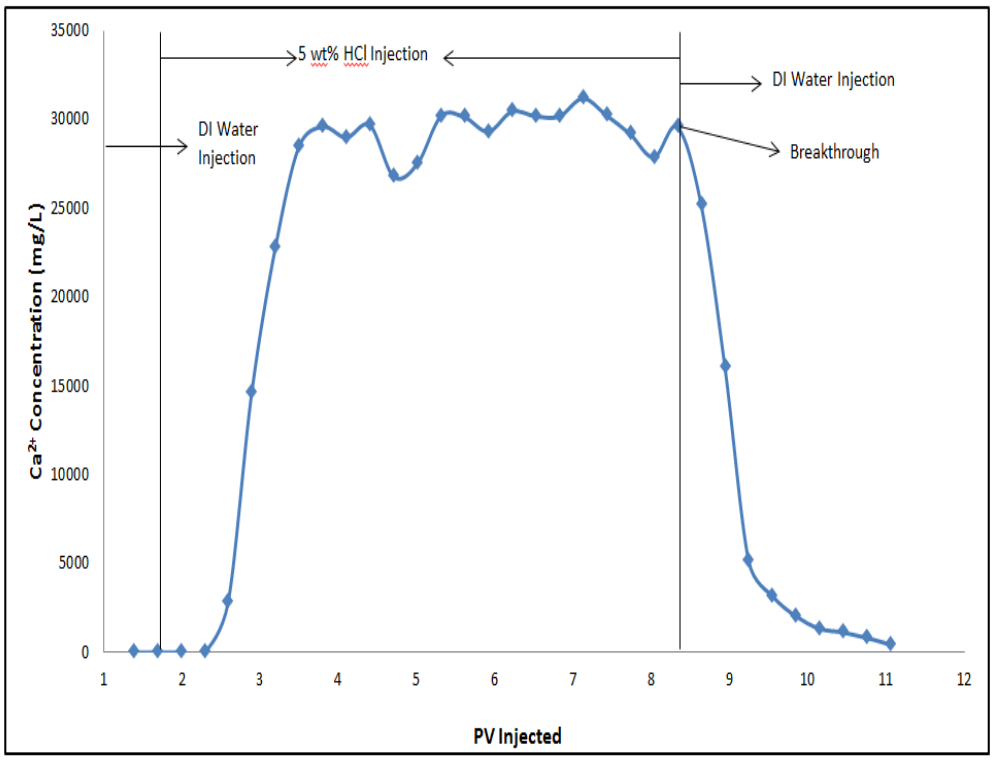

Figure III.18: Calcium ion concentration in acid injection effluent for Experiment 2

Calcium ion concentration in the effluent starts increasing after 0.6 pore volumes of acid were injected. The concentration then fluctuates between 26,800 and 31,200 mg/L for the duration of the acid injection. Calcium ion concentration decreases sharply after the breakthrough is reached as injection is switched to DI water. A summary of the results of Experiment 3 are displayed in Table 3.4.

Experiment 3: 20 inch Indiana limestone core with 5 wt.% HCl

Table III.4: Summary of Results for Experiment 3

Core Name	B1-6
Pre-acidizing Porosity (%)	14.18
Pre-acidizing Pore Volume (cm3)	82.1
Pre-acidizing Permeability (md)	14.1
Post-acidizing Porosity (%)	17.75
Dissolved Matrix (g)	20.71
Pore Volume to Breakthrough	1.12

Figures 3.19, 3.20, 3.21, and 3.22 are photographs of the core sample's inlet and outlet, before and after acid injection respectively.

Figure III.19: B1-6 inlet before acid injection

Figure III.20: B1-6 outlet before acid injection

Figure III.21: B1-6 inlet after acid injection

Figure III.22: B1-6 outlet after acid injection

After acid injection, some dissolution of the matrix at the outside surface of the core was observed. This dissolution marks points where the acid broke through

prematurely but was forced to continue lengthwise along the core axis by the rubber sleeve surrounding the core. This is displayed in Figure 3.23.

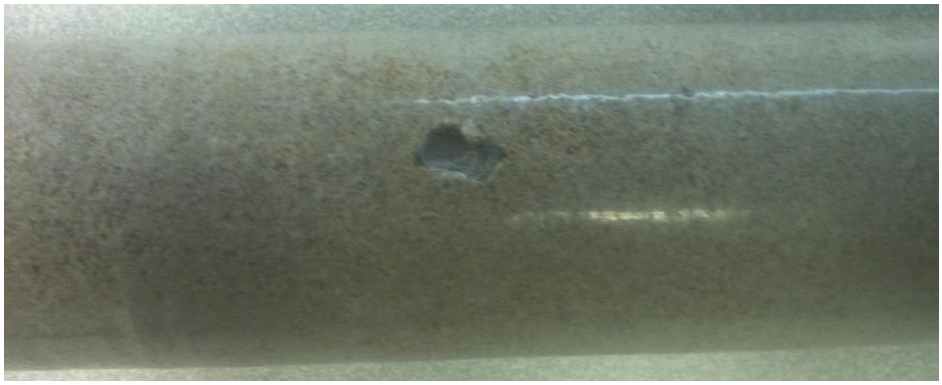

Figure III.23: Surface dissolution on B1-6 after acid injection

Some dissolution can be observed at the inlet side of the core. This implies that for 15 wt% HCl injected at 5 cm^3/min, once the wormholing has begun the flow rate is slow enough to cause slight face dissolution. The wormhole can be observed at the outlet where the acid broke through. Figures 3.24 and 3.25 show CT scans of the core sample before and after acid injection respectively.

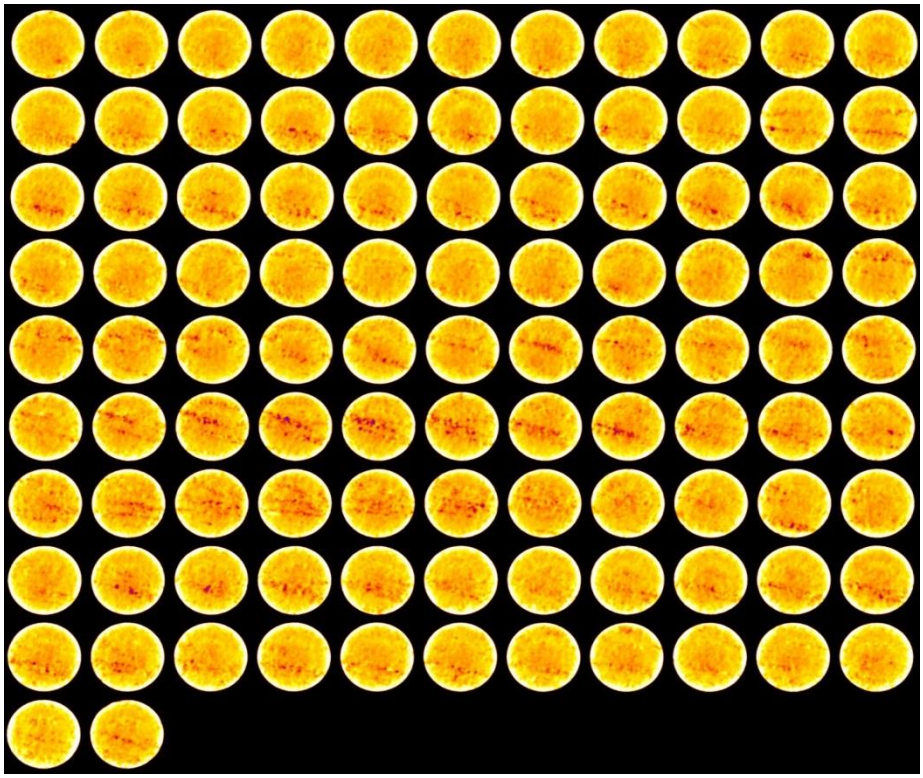

Figure III.24: CAT scan of B1-6 before acid injection

Some vugs are observed in the core (red patches), correlating with its high permeability. This vuginess is mainly concentrated in the center of the core. Some white patches are observed in the core sample, which could indicate a slight degree of dolomitazation.

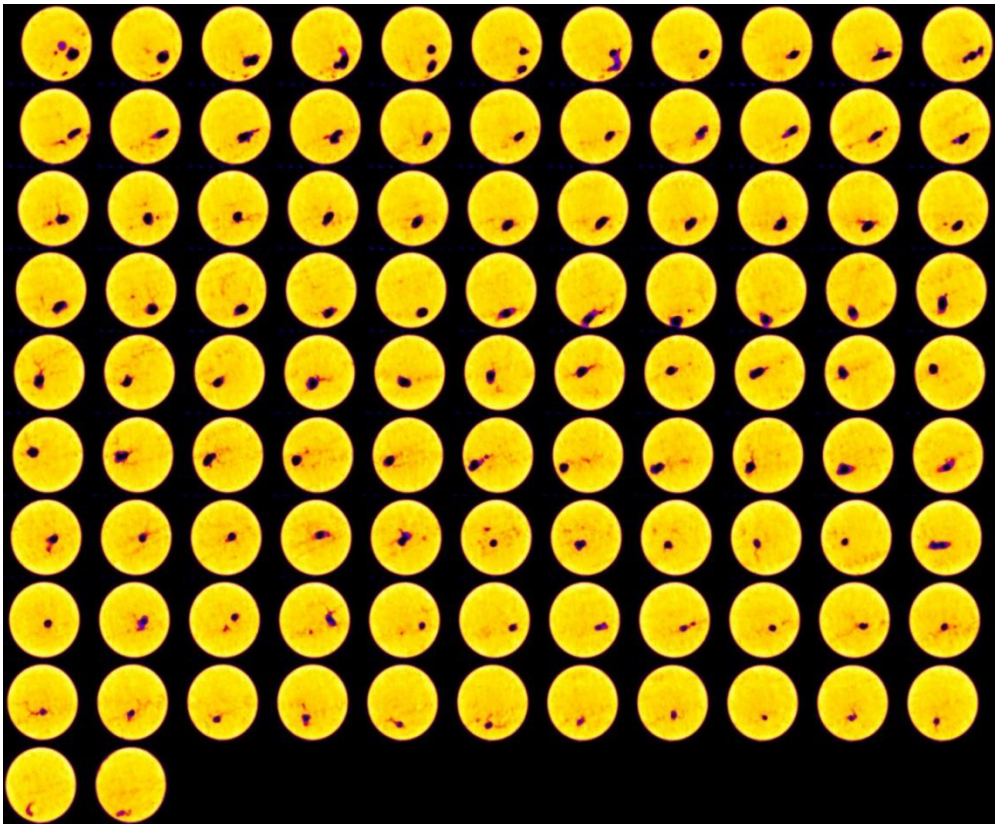

Figure III.25: CAT scan of B1-6 after acid injection

The propagation of the acid-induced wormholes can be observed in the previous image. The wormholing closer to the inlet is larger than that closer to the outlet. As the acid propagates deeper into the core, it spends as it reacts with the walls of the wormholes. There is less live acid reaching the tip of the wormhole deeper into the core compared to the inlet. Therefore the acid attack becomes progressively less aggressive and the size of the wormhole becomes smaller. Figure 3.26 displays the pressure drop across the core sample during the acid injection procedure.

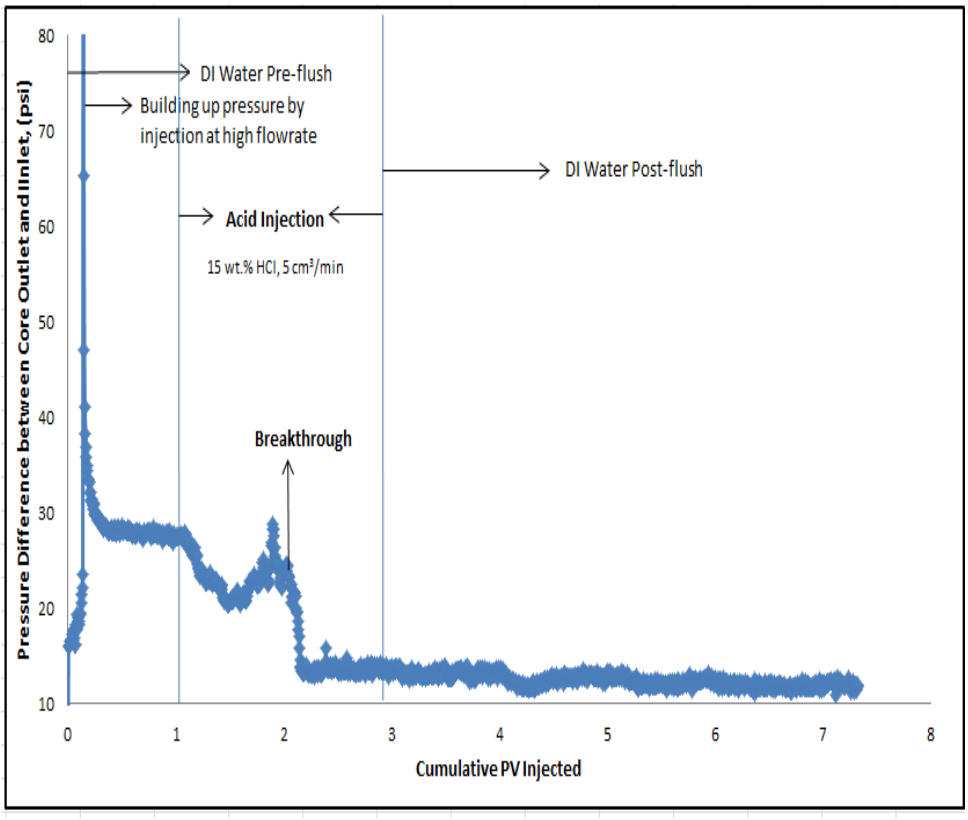

Figure III.26: Pressure drop across the core sample for Experiment 3

The pressure difference continues to decrease after acid injection due to wormhole formation as the acid dissolves the matrix. Acid injection ends and DI water flush starts at cumulative PV of 2.8. The breakthrough occurs after 1.12 pore volumes of acid were injected. HCl concentration in the effluent samples was measured using an auto-titration machine. For all the effluent samples collected, the concentration of live acid was zero. This is due to the reactive nature of the acid (spending along the wormhole) and the switch to DI water promptly after breakthrough. Figure 3.27 displays the concentration of calcium ions versus the cumulative pore volumes injected.

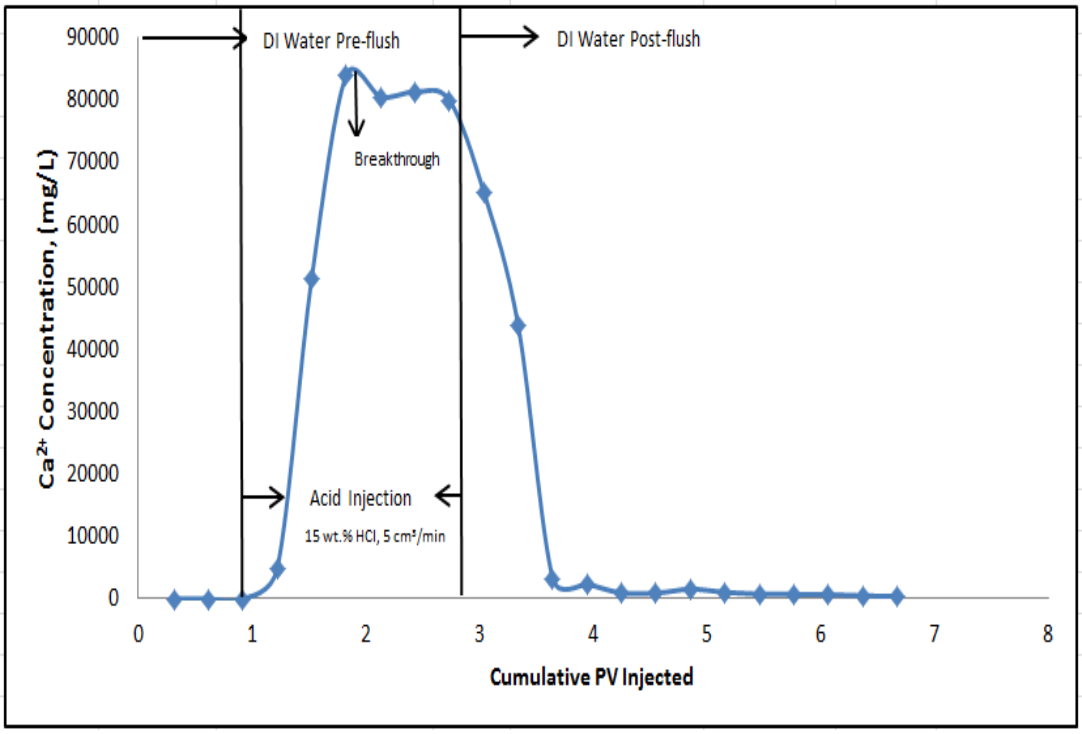

Figure III.27: Calcium ion concentration in acid injection effluent for Experiment 3

Calcium ion concentration in the effluent starts increasing after the switch to acid injection. The concentration rises then fluctuates between 83,930 and 79,710 mg/L for the duration of the acid injection. Calcium ion concentration decreases after the injection is switched to DI water and returns to zero. Table 3.5 summarizes the main results from Experiment 4.

Experiment 4: 20 inch Indiana limestone core with 5 wt.% HCl at 1850 psi backpressure

Table III.5: Summary of Results for Experiment 4

Core Name	B1-9
Pre-acidizing Porosity (%)	13.46
Pre-acidizing Pore Volume (cm3)	77.96
Pre-acidizing Permeability (md)	95.3
Post-acidizing Porosity (%)	19.37
Dissolved Matrix (g)	34.25
Pore Volume to Breakthrough	5.26

Figures 3.28, 3.29, 3.30, and 3.31 are photographs of the core sample's inlet and outlet, before and after acid injection respectively.

Figure III.28: B1-9 inlet before acid injection

Figure III.29: B1-9 outlet before acid injection

Figure III.30: B1-9 inlet after acid injection

Figure III.31:B1-9 outlet after acid injection

After acid injection, some dissolution of the matrix at the outside surface of the core was observed. This dissolution marks points where the acid broke through prematurely but was forced to continue lengthwise along the core axis by the rubber sleeve surrounding the core. This is displayed in Figure 3.23.

Figure III.32: B1-9, displayed lengthwise, after acid injection

Just as in Experiment 2, face dissolution can be observed at the inlet, in addition to a large wormhole size. This implies that for 5 wt% HCl injected at 5 cm^3/min, once the wormholing has begun the flow rate is slow enough to cause face dissolution and enlarge the formed wormhole. The wormhole can be observed at the outlet where the acid broke through. Figures 3.33 and 3.34 show CT scans of the core sample before and after acid injection respectively.

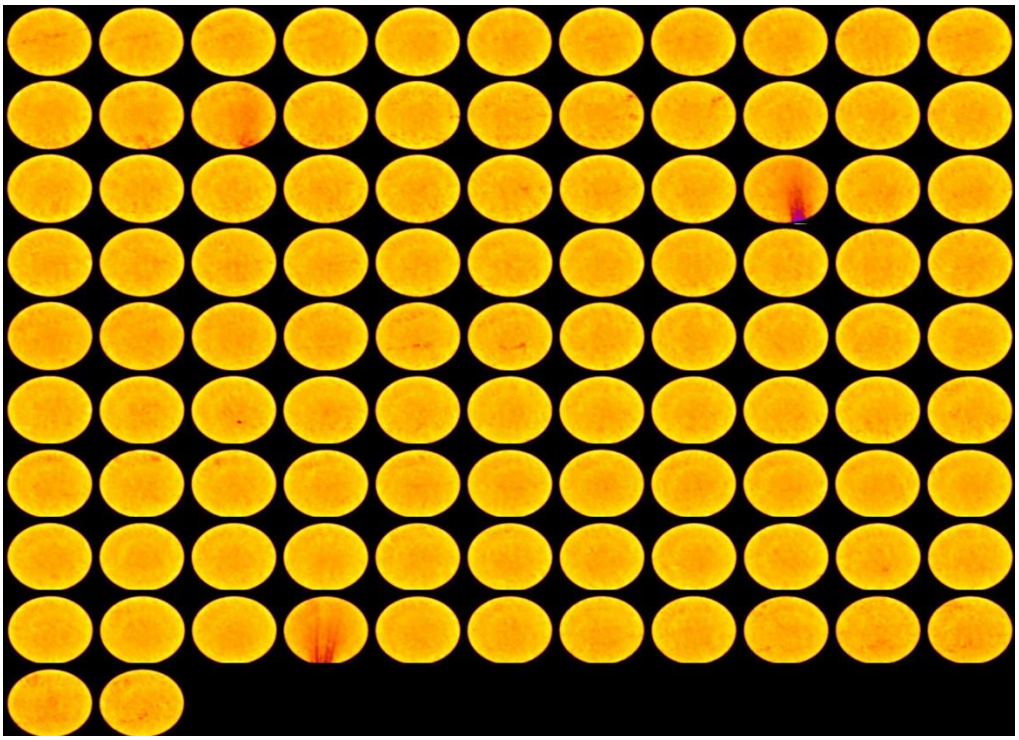

Figure III.33: CAT scan of B1-9 before acid injection

The figure above indicates the presence of some vugs in the core sample (red patches), correlating with its high permeability. The lithology of the core sample appears to be homogenous; there are no major solid white patches or streaks appearing in the bulk of the core sample.

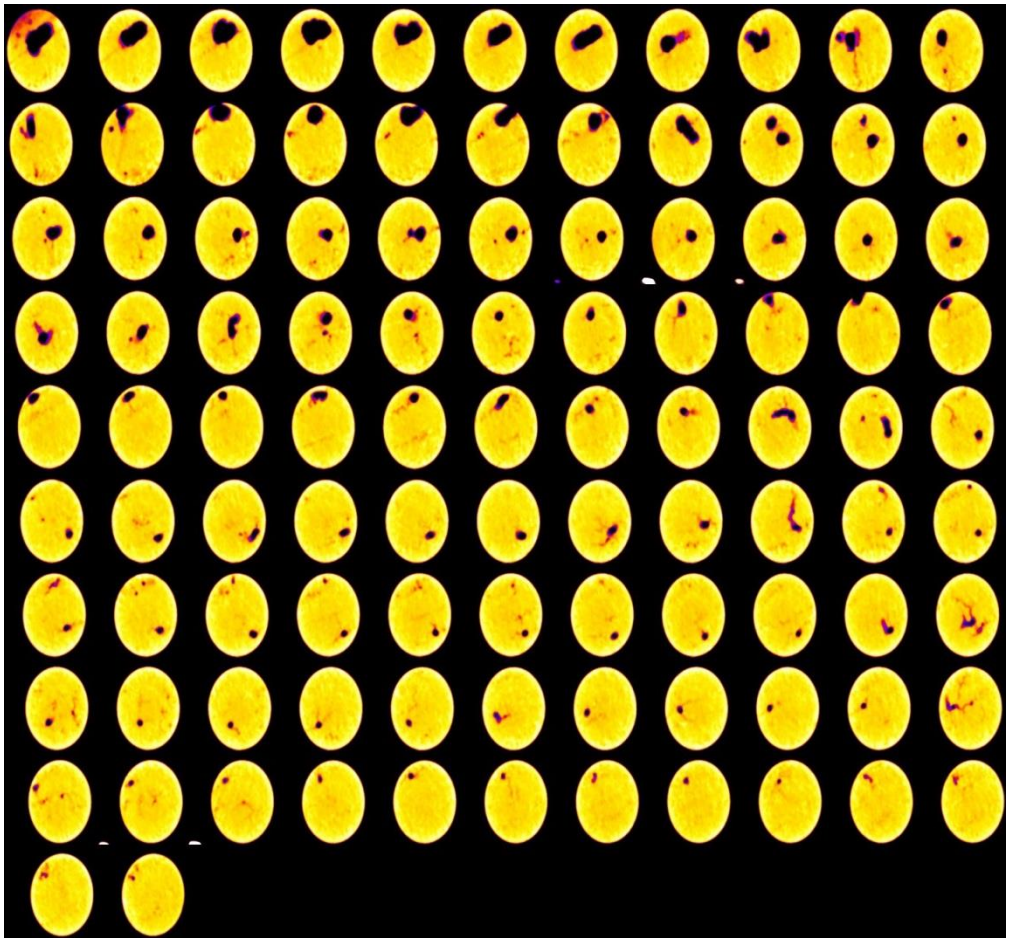

Figure III.34: CAT scan of B1-9 after acid injection

The propagation of the acid-induced wormholes can be observed in the previous figure. The wormholes closer to the inlet are much larger than those closer to the outlet. As the acid propagates deeper into the core, it spends as it reacts with the walls of the wormholes. Also, there is less live acid reaching the tip of the wormhole deeper into the core compared to the inlet. Therefore the acid attack becomes progressively less aggressive and the size of the wormhole becomes progressively smaller. Figure 3.35 displays the pressure drop across the core sample during the acid injection procedure.

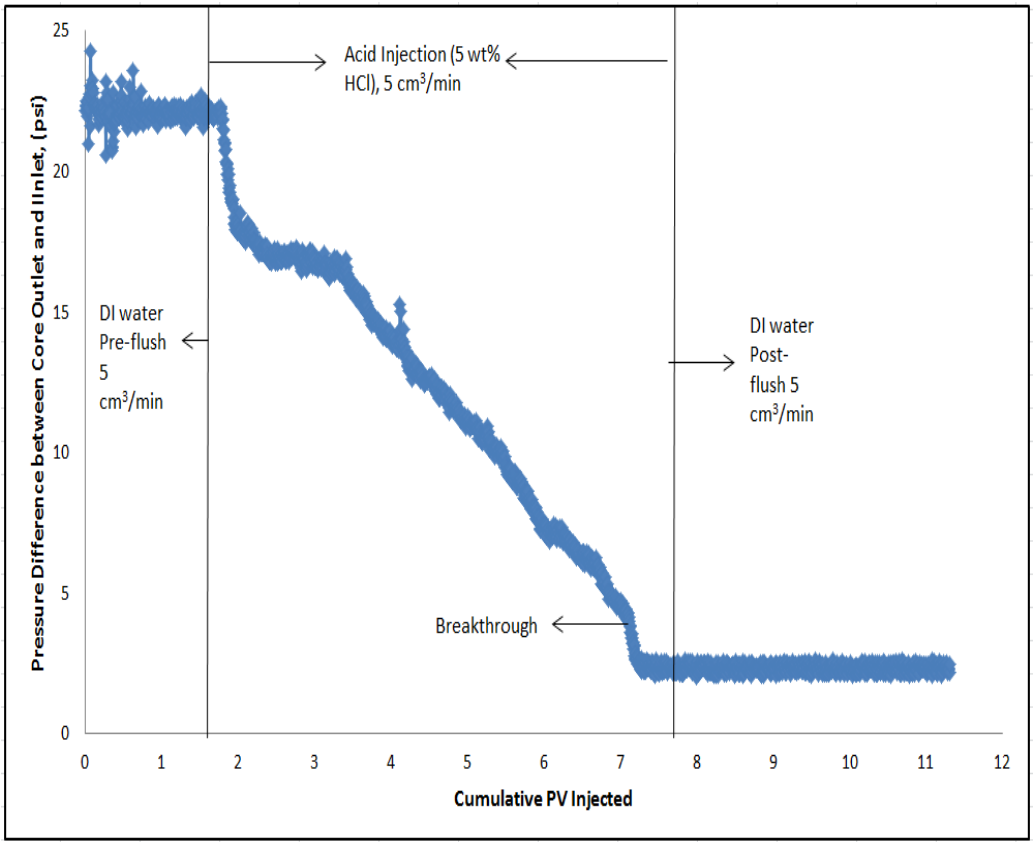

Figure III.35: Pressure drop across core sample for Experiment 4

The pressure difference starts to decrease after acid injection due to wormhole formation as the acid dissolves the matrix. Acid injection ends and DI water flush starts at PV of 7.76. The breakthrough occurs after 5.26 pore volumes of acid were injected. HCl concentration in the effluent samples was measured using an auto-titration machine. For all the effluent samples collected, the concentration of live acid was zero. This is due to the reactive nature of the acid (spending along the wormhole) and the switch to DI water promptly after breakthrough.

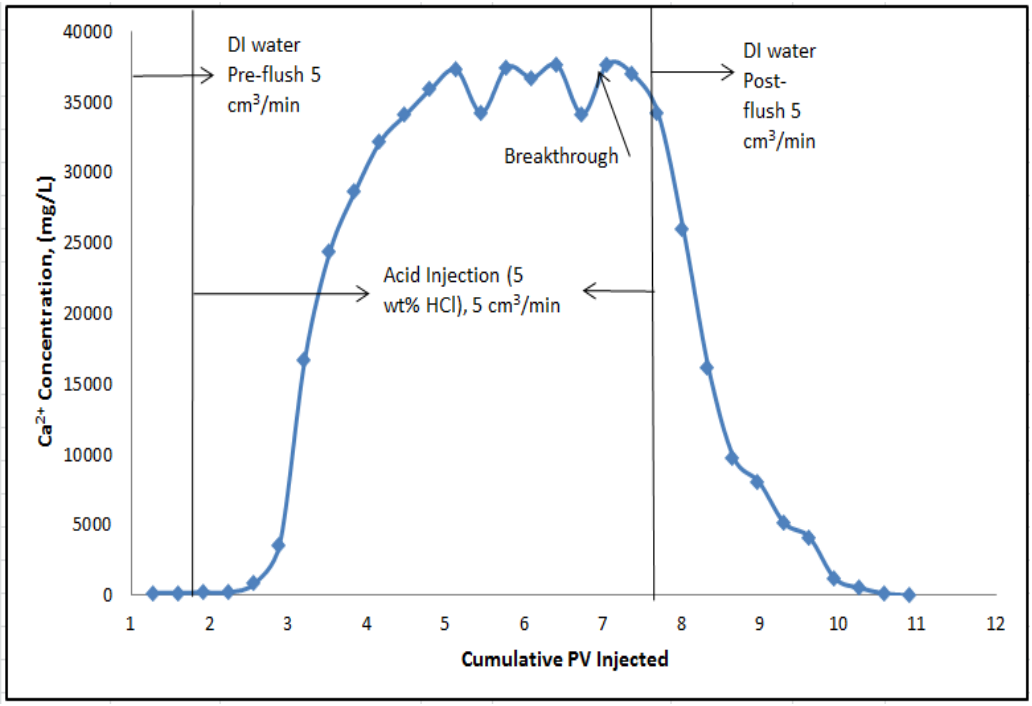

Figure III.36: Calcium ion concentration in acid injection core effluent

Figure 3.36 shows the concentration of calcium ions versus the cumulative pore volumes injected. Calcium ion concentration in the effluent starts increasing after 1.2 pore volumes of acid were injected. The concentration then rises and fluctuates between 34,120 and 37,590 mg/L for the duration of the acid injection. Calcium ion concentration decreases sharply after the breakthrough is reached and injection is switched to DI water.

CHAPTER IV

INVESTIGATING THE EFFECTS OF ACID FLOWRATE ON PVBT IN 20 INCH INDIANA LIMESTONE CORES

As in the previous chapter, Chapter IV is divided into two parts. In the first part, titled "Experimental Plan", the laboratory tests performed to evaluate the effect of core length on PVBT are outlined. The experimental procedure that is employed in these tests is also described. In the second part, titled "Results and Discussion", the results of each experiment are presented and the immediate significance of the findings is discussed. A more detailed treatment of the results and more comparative analysis are included in Chapter VI.

EXPERIMENTAL PLAN

The following experiments, displayed in Table 4.1, were performed to evaluate the effects of core length on PVBT in Indiana limestone cores. All experiments were performed on 20 inch cores and at a temperature of 150 °F. The HCl solution concentration was 15 percent by weight for all experiments.

Table IV.1: Experimental Outline for Chapter IV

Experiment Number	Core Name	Acid Injection Flowrate (cm^3/min)	Backpressure (psi)
5	B3-1	5	1850
6	B3-2	10	1000
7	B3-3	20	1850
8	B3-4	10	1850
9	B3-5	20	1000

The procedure employed to prepare the core samples used in these experiments is identical to the procedure described in Chapter III. The procedures for acid injection and post-injection analysis (ICP, titration, porosity, and dissolved rock) are also identical.

RESULTS AND DISCUSSION

The results of Experiment 5 are displayed in Table 4.2.

Experiment 5: Core treated with 15 wt.% HCl at 5 cm^3/min and 1850 psi backpressure

Table IV.2: Summary of Results for Experiment 5

Core Name	B3-1
Pre-acidizing Porosity (%)	12.09
Pre-acidizing Pore Volume (cm3)	70
Pre-acidizing Permeability (md)	22.2
Post-acidizing Porosity (%)	12.38
Dissolved Matrix (g)	1.7
Pore Volume to Breakthrough	0.2

Figures 4.1, 4.2, 4.3, and 4.4 are photographs of the core sample's inlet and outlet, before and after acid injection respectively.

Figure IV.1: B3-1 inlet before acid injection

Figure IV.2: B3-1 outlet before acid injection

Figure IV.3: B3-1 inlet after acid injection

Figure IV.4: B-1 outlet after acid injection

After acid injection, some dissolution of matrix at the outside surface of the core was observed. This dissolution marks points where the acid broke through prematurely and caused wormholing on the outer surface of the core. This is displayed in Figures 4.5 and 4.6.

Figure IV.5: B3-1, displayed lengthwise, after acid injection

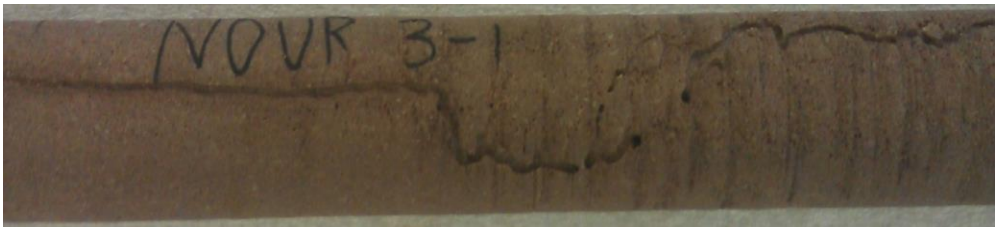

Figure IV.6: Surface dissolution across B3-1 after acid injection

The surface wormholing continues till the wormhole reaches the outlet. The wormhole can be observed at the outlet where the acid broke through. Figure 4.7 displays the pressure drop across the core sample during the acid injection procedure.

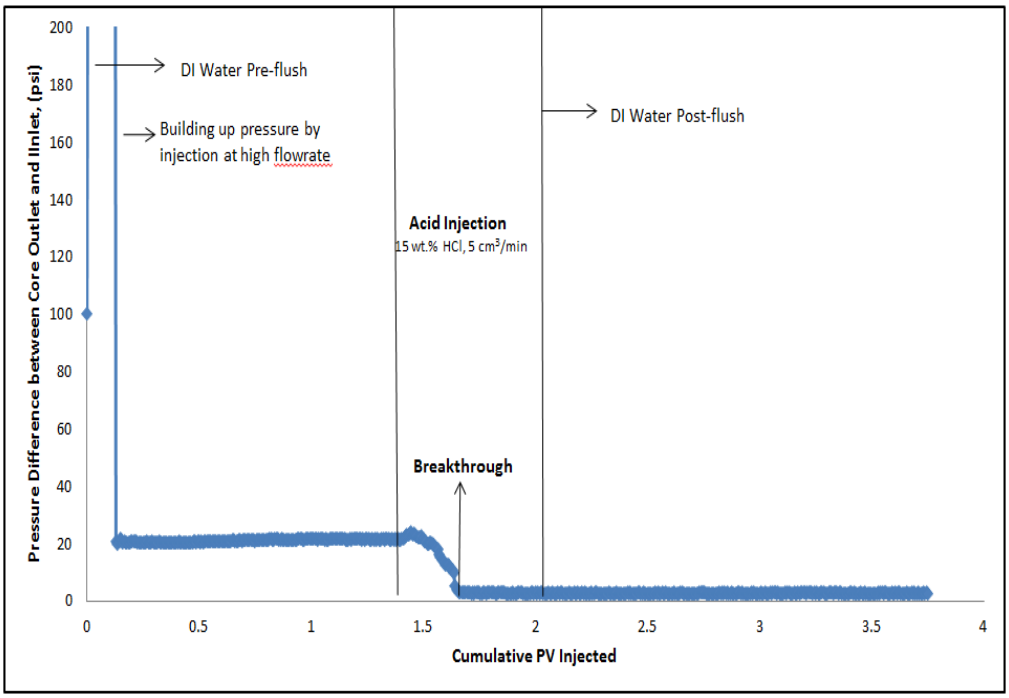

Figure IV.7: Pressure drop across core sample for Experiment 5

Before acid injection, the flowrate and temperature were allowed to stabilize using DI water at 150°F and 5 cm^3/min. The breakthrough is labeled on the above figure. The slight increase in pressure difference after the switch to acid injection is due to the higher viscosity of the acid solution. The acid injection ends and DI water flush starts at cumulative PV of 2, and the breakthrough occurs after **0.2** pore volumes of acid were injected. HCl concentration in the effluent samples was measured using an auto-titration machine. For all the effluent samples collected, the concentration of live acid was zero. This is due to the reactive nature of the acid (spending along the wormhole) and switch to DI water promptly after breakthrough. Figure 4.8 displays the concentration of calcium ions versus the cumulative pore volumes injected.

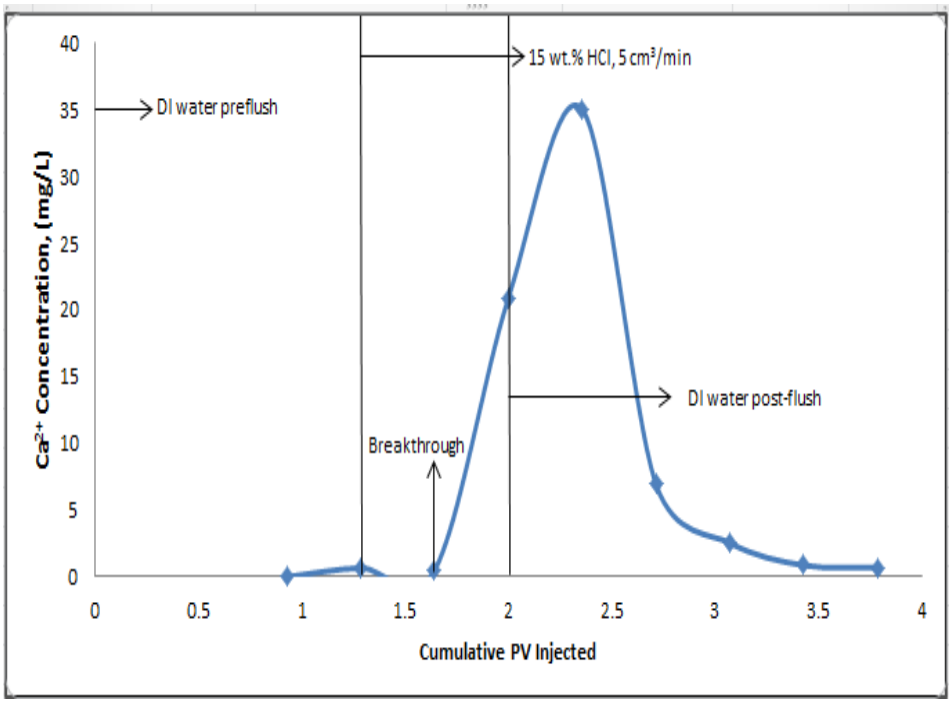

Figure IV.8: Calcium ion concentration in acid injection effluent for Experiment 5

Calcium ion concentration in the effluent starts increasing after the switch to acid injection. The concentration rises then reaches a maximum of 35 mg/L after breakthrough. Calcium ion concentration decreases sharply after the peak to 5 mg/L then gradually to zero. The results of Experiment 6 are presented in Table 4.3.

Experiment 6: Core treated with 15 wt.% HCl at 10 cm^3/min and 1000 psi backpressure

Table IV.3: Summary of Results for Experiment 6

Core Name	B3-2
Pre-acidizing Porosity (%)	14.45
Pre-acidizing Pore Volume (cm3)	83.67
Pre-acidizing Permeability (md)	139.3
Post-acidizing Porosity (%)	14.88
Dissolved Matrix (g)	2.5
Pore Volume to Breakthrough	0.5

Figures 4.9, 4.10, 4.11, and 4.12 are photographs of the core sample's inlet and outlet, before and after acid injection respectively.

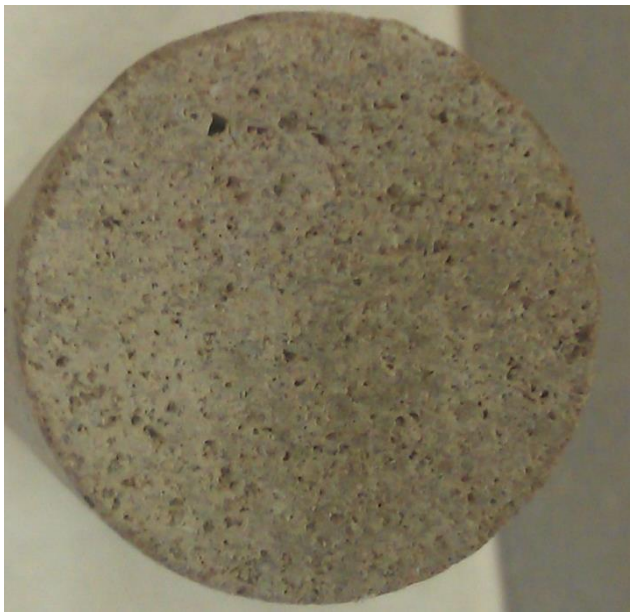

Figure IV.9: : B3-2 inlet before acid injection

Figure IV.10: B3-2 outlet before acid injection

Figure IV.11: B3-2 inlet after acid injection

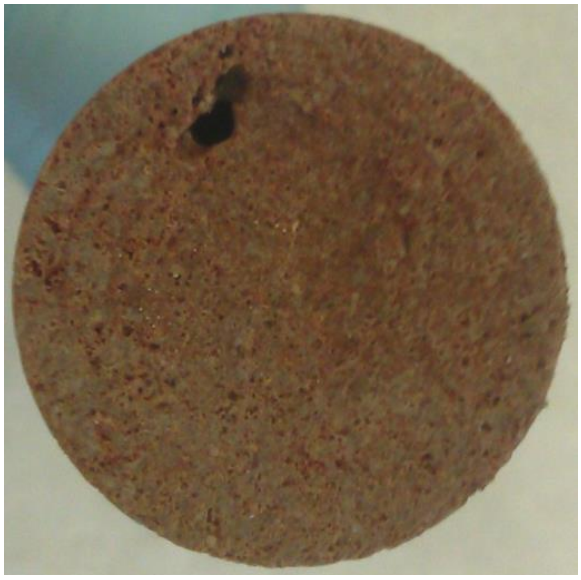

Figure IV.12: B3-2 outlet after acid injection

After acid injection, some dissolution of matrix at the outside surface of the core was observed. This dissolution marks points where the acid broke through prematurely and caused wormholing on the outer surface of the core. This is displayed in Figures 4.13 and 4.14.

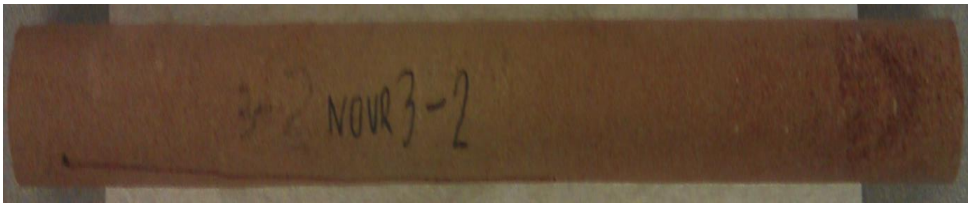

Figure IV.13: B3-2, displayed lengthwise, after acid injection

Figure IV.14: B3-2, displayed lengthwise, after acid injection

The surface wormholing continues till the wormhole reaches the outlet. The wormhole can be observed at the outlet where the acid broke through. . Figure 4.15 displays the pressure drop across the core sample during the acid injection procedure.

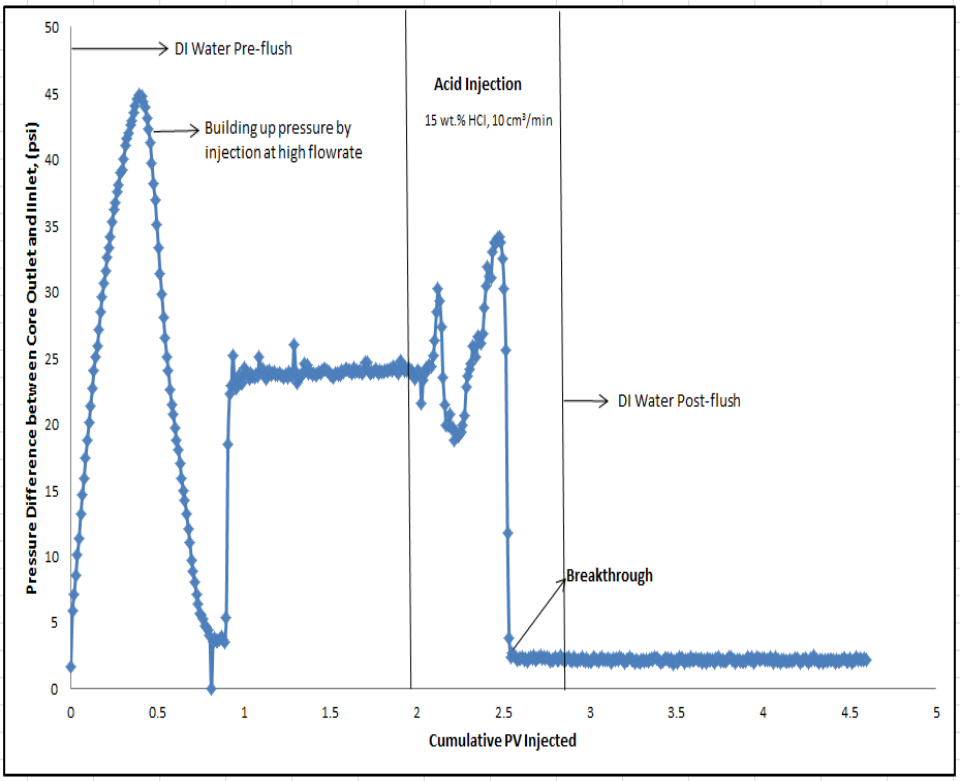

Figure IV.15: Pressure drop across core sample for Experiment 6

Before acid injection, the flowrate and temperature were allowed to stabilize using DI water at 150°F and 10 cm^3/min. The breakthrough is labeled on the figure above. The increase in pressure difference after switch to acid injection is due to higher viscosity of acid solution. Acid injection ends and DI water flush starts at cumulative PV of 2.8. The breakthrough occurs after **0.5** pore volumes of acid were injected. HCl concentration in the effluent samples was measured using an auto-titration machine. For all the effluent samples collected, the concentration of live acid was zero. This is due to the reactive nature of the acid and switch to DI water promptly after breakthrough. Figure 4.16 displays the concentration of calcium ions versus the cumulative pore volumes injected.

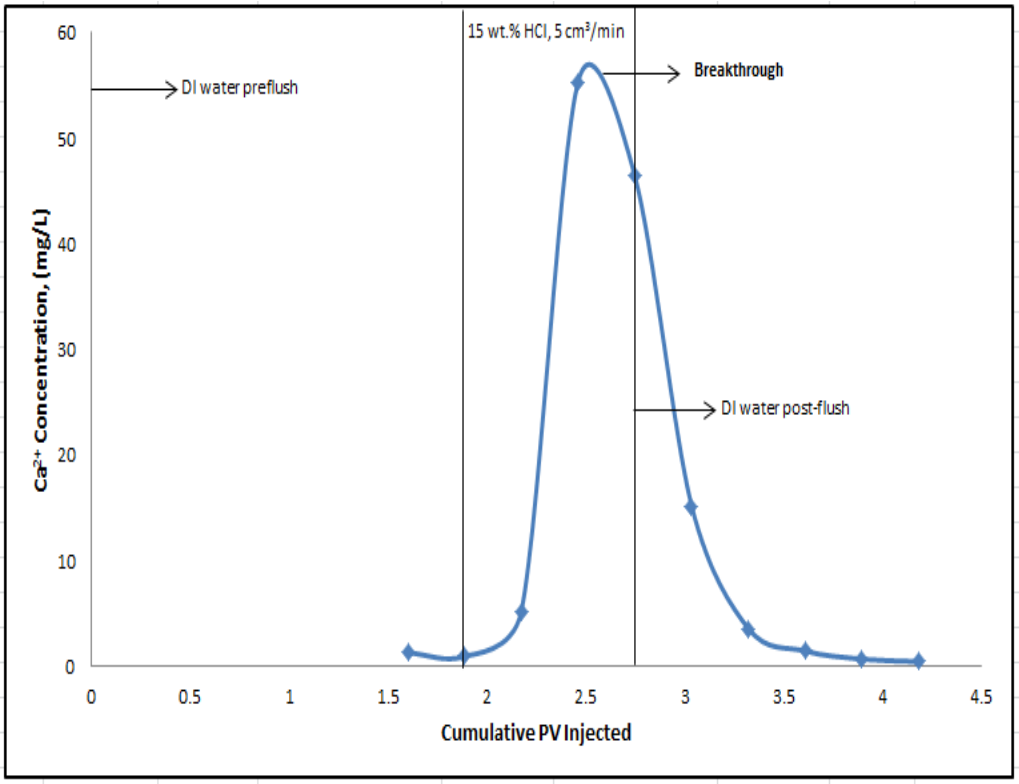

Figure IV.16: Calcium ion concentration in acid injection effluent for Experiment 6

Calcium ion concentration in the effluent starts increasing after the switch to acid injection. The concentration rises then reaches a maximum of 55 mg/L before breakthrough. Calcium ion concentration decreases sharply after the peak to 3.5 mg/L then gradually to zero. The results of Experiment 7 are presented in Table 4.4.

Experiment 7: Core treated with 15 wt.% HCl at 20 cm^3/min and 1850 psi backpressure

Table IV.4: Summary of Results for Experiment 7

Core Name	B3-3
Pre-acidizing Porosity (%)	16.4
Pre-acidizing Pore Volume (cm3)	94.88
Pre-acidizing Permeability (md)	135.3
Post-acidizing Porosity (%)	17.7
Dissolved Matrix (g)	7.6
Pore Volume to Breakthrough	0.7

Figures 4.17, 4.18, 4.19, and 4.20 are photographs of the core sample's inlet and outlet, before and after acid injection respectively.

Figure IV.17: B3-3 inlet before acid injection

Figure IV.18: B3-3 outlet before acid injection

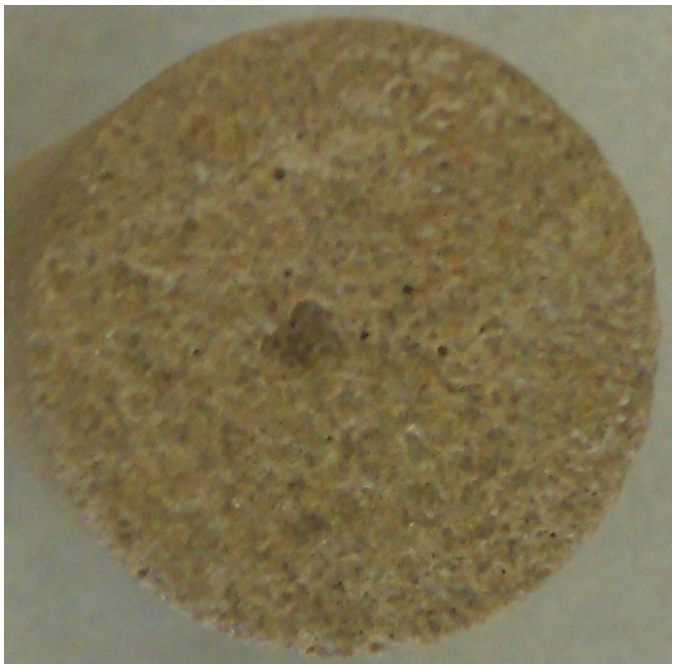

Figure IV.19: B3-3 inlet after acid injection

Figure IV.20: B3-3 outlet after acid injection

After acid injection, some dissolution of matrix at the outside surface of the core was observed. This dissolution marks points where the acid broke through prematurely and caused wormholing on the outer surface of the core. This is displayed in Figure 4.21.

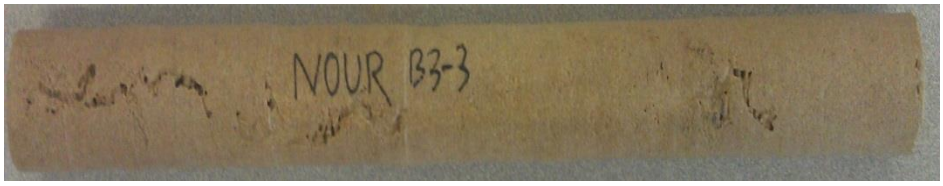

Figure IV.21: B3-3, displayed lengthwise, after acid injection

The surface wormholing continues till the wormhole reaches the outlet. The wormhole can be observed at the outlet where the acid broke through. Figure 4.22 displays the pressure drop across the core sample during the acid injection procedure.

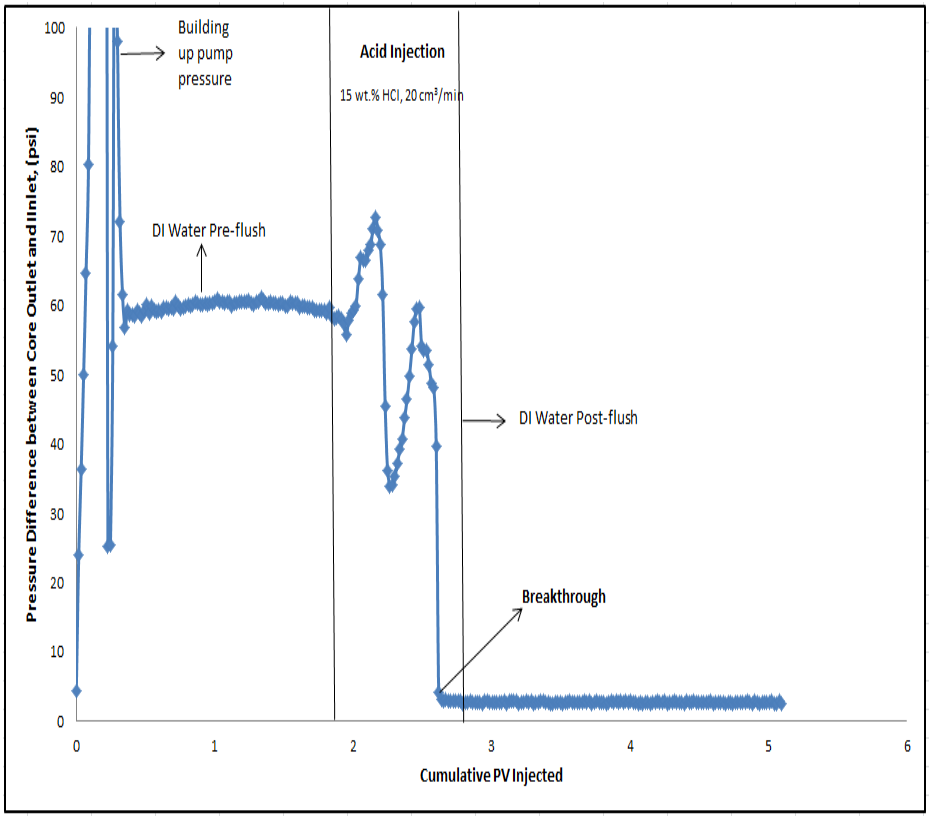

Figure IV.22: Pressure drop across core sample for Experiment 7

Before acid injection, the flowrate and temperature were allowed to stabilize using DI water at 150°F and 20 cm^3/min. The breakthrough is labeled on the figure above. The increase in pressure difference after switching to acid injection is due to the higher viscosity of acid solution. Acid injection ends and DI water flush starts at cumulative PV of 2.7. The breakthrough occurs after **0.7** pore volumes of acid were injected. HCl concentration in the effluent samples was measured using an auto-titration machine. For all the effluent samples collected, the concentration of live acid was zero. This is due to the reactive nature of the acid and switch to DI water promptly after

breakthrough. Figure 4.23 displays the concentration of calcium ions versus the cumulative pore volumes injected.

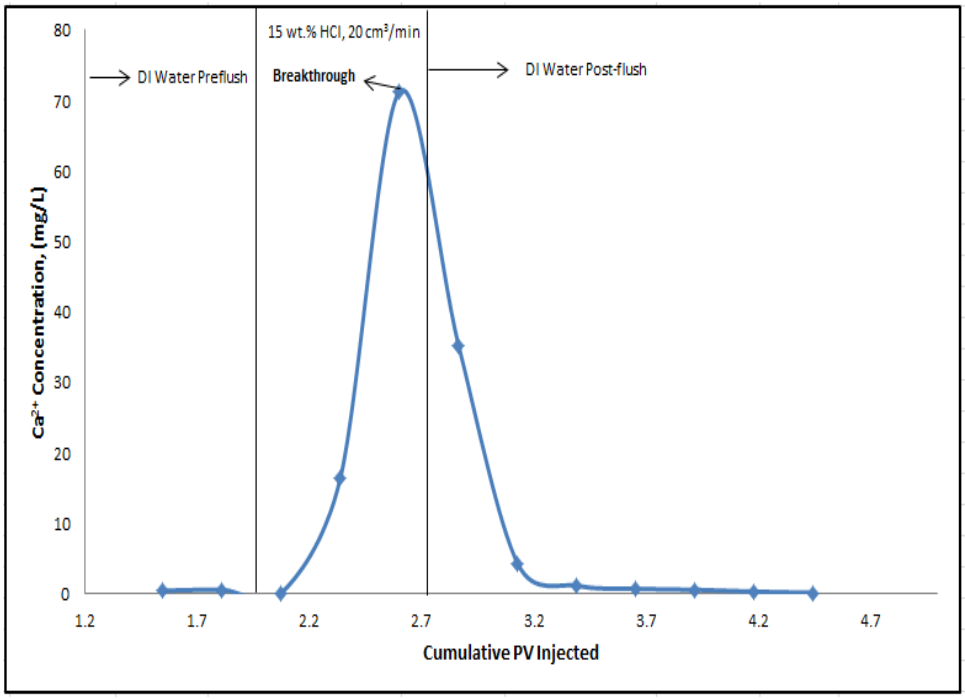

Figure IV.23: Calcium ion concentration in acid injection effluent for Experiment 7

Calcium ion concentration in the effluent starts increasing after the switch to acid injection. The concentration rises then reaches a maximum of 70 mg/L before breakthrough. Calcium ion concentration decreases sharply to 4 mg/L after switching to water injection then gradually decreases to zero. The results of Experiment 8 ate presented in Table 4.5.

Experiment 8: Core treated with 15 wt.% HCl at 10 cm^3/min and 1850 psi backpressure

Table IV.5: Summary of Results for Experiment 8

Core Name	B3-4
Pre-acidizing Porosity (%)	14.73
Pre-acidizing Pore Volume (cm3)	85.3
Pre-acidizing Permeability (md)	125.2
Post-acidizing Porosity (%)	19.4
Dissolved Matrix (g)	27
Pore Volume to Breakthrough	1.22

Figures 4.24, 4.25, 4.26, and 4.27 are photographs of the core sample's inlet and outlet, before and after acid injection respectively.

Figure IV.24: B3-4 inlet before acid injection

Figure IV.25: B3-4 outlet before acid injection

Figure IV.26: B3-4 inlet after acid injection

Figure IV.27: B3-4 outlet after acid injection

The above figures show the wormholing at the core inlet and outlet after acid injection.

A higher degree of face dissolution is observed at the core inlet after acid injection. This

is because an excess of acid was injected even after breakthrough was reached (refer to the discussion after Figure 4.28 displayed below). Figure 4.28 displays the pressure drop across the core sample during the acid injection procedure.

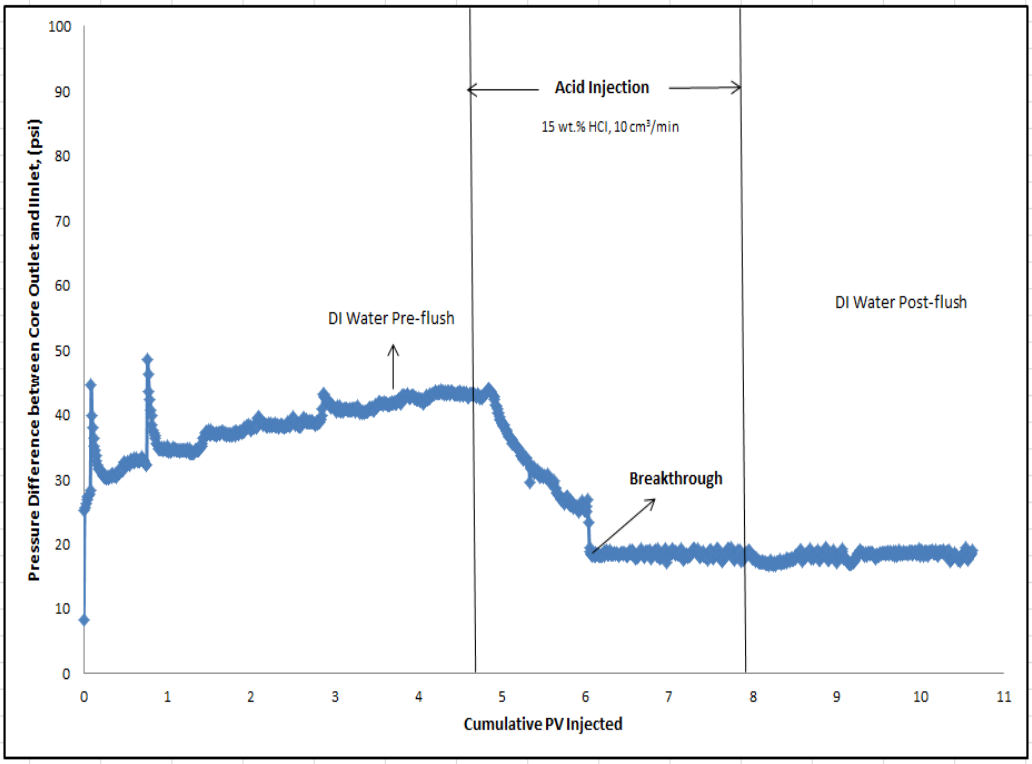

Figure IV.28: Pressure drop across core sample for Experiment 8

Before acid injection, the flowrate and temperature were allowed to stabilize using DI water at 150°F and 10 cm^3/min. The breakthrough is labeled on the figure above. The acid injection ends and the DI water flush starts at cumulative PV of 7.8. The breakthrough occurs after **1.22** pore volumes of acid were injected. After breakthrough, an excess of almost 2 pore volumes of acid was injected. The excess acid was injected due to uncertainty on whether the breakthrough was reached. The uncertainty was

because the pressure drop was abnormally high even after breakthrough (17 psi). The Breakthrough was confirmed via visual inspection after the experiment.

HCl concentration in the effluent samples was measured using an auto-titration machine. For all the effluent samples collected, the concentration of live acid was zero. This is due to the reactive nature of the acid and switch to DI water promptly after breakthrough. Figure 4.29 displays the concentration of calcium ions versus the cumulative pore volumes injected.

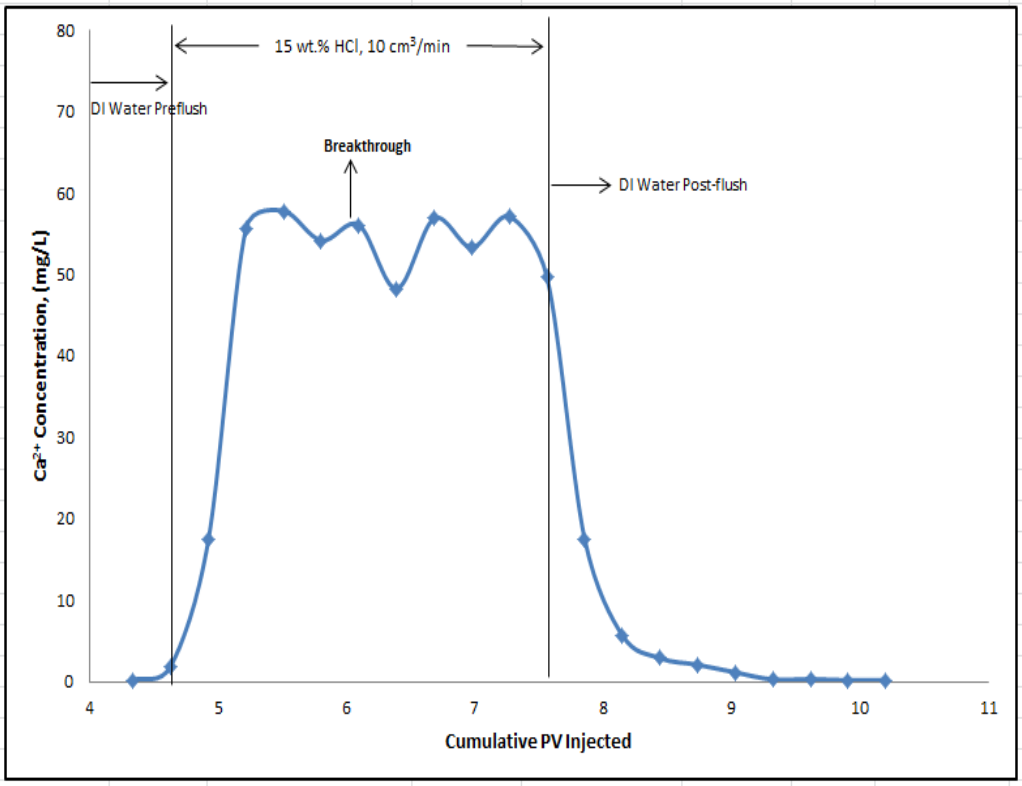

Figure IV.29: Calcium ion concentration in acid injection effluent for Experiment 8

Calcium ion concentration in the effluent starts increasing after the switch to acid injection. The concentration ranges around the 55 mg/L mark throughout acid injection.

Calcium ion concentration decreases sharply after the switch to water and then gradually reaches zero. The results of Experiment 9 are presented in Table 4.6.

Experiment 9: Core treated with 15 wt.% HCl at 20 cm^3/min and 1000 psi backpressure

Table IV.6: Summary of Results for Experiment 9

Core Name	B3-5
Pre-acidizing Porosity (%)	14.8
Pre-acidizing Pore Volume (cm3)	85.7
Pre-acidizing Permeability (md)	89.5
Post-acidizing Porosity (%)	15.6
Dissolved Matrix (g)	4.7
Pore Volume to Breakthrough	0.53

Figures 4.30, 4.31, 4.32, and 4.33 are photographs of the core sample's inlet and outlet, before and after acid injection respectively.

Figure IV.30: B3-5 inlet before acid injection

Figure IV.31: B3-5 outlet before acid injection

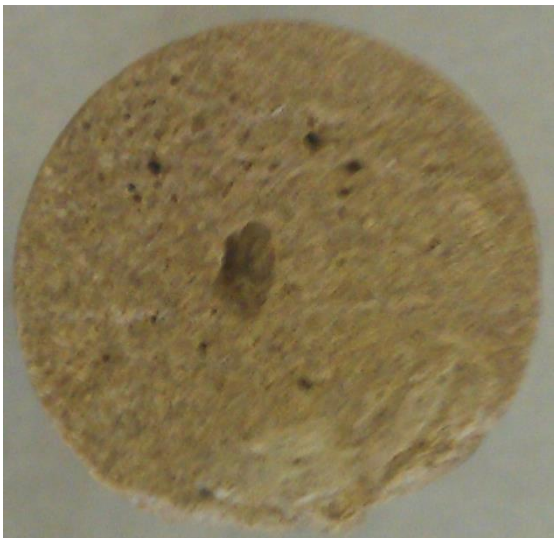

Figure IV.32: B3-5 inlet after acid injection

Figure IV.33: B3-5 outlet after acid injection

After acid injection, some dissolution of matrix at the outside surface of the core was observed. This dissolution marks points where the acid broke through prematurely and caused wormholing on the outer surface of the core. This is displayed in Figure 4.34.

Figure IV.34: B3-5, displayed lengthwise, after acid injection

The surface wormholing continues till the wormhole reaches the outlet. The wormhole can be observed at the outlet where the acid broke through. Figure 4.35 displays the pressure drop across the core sample during the acid injection procedure.

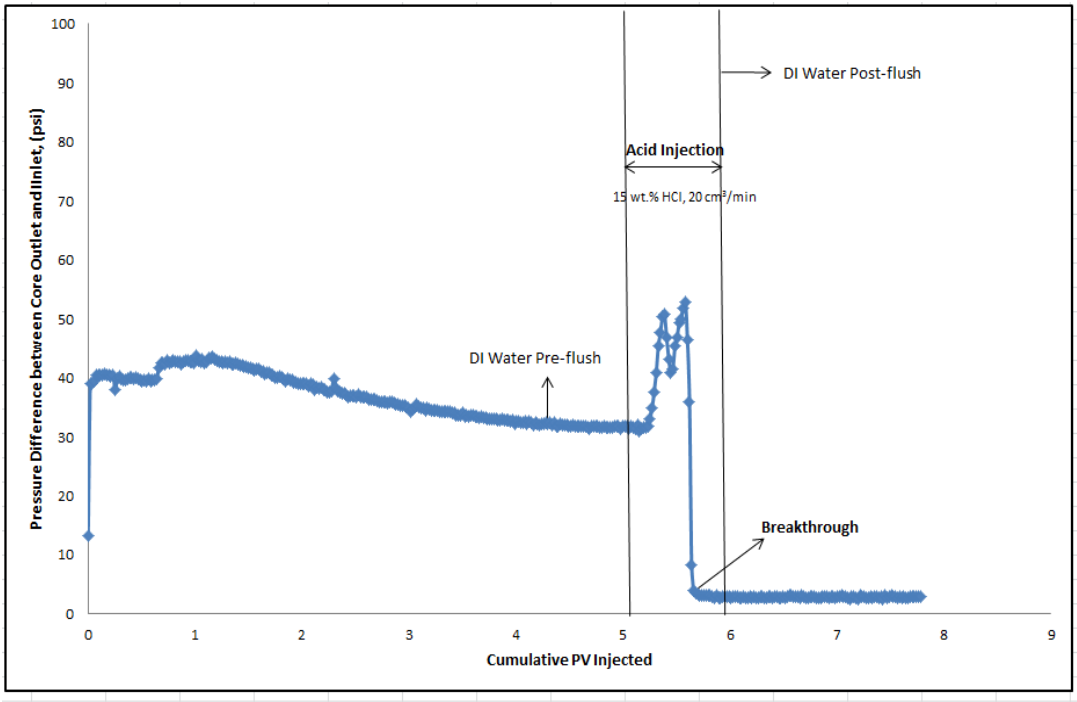

Figure IV.35: Pressure drop across core sample for Experiment 9

Before acid injection, the flowrate and temperature were allowed to stabilize using DI water at 150°F and 20 cm^3/min. The breakthrough is labeled on the figure above. The increase in pressure difference after the switch to acid injection is due to the higher viscosity of acid solution. Acid injection ends and DI water flush starts at cumulative PV of 5.8. The breakthrough occurs after **0.53** pore volumes of acid were injected.

HCl concentration in the effluent samples was measured using an auto-titration machine. For all the effluent samples collected, the concentration of live acid was zero. This is due to the reactive nature of the acid and switch to DI water promptly after breakthrough. Figure 4.36 displays the concentration of calcium ions versus the cumulative pore volumes injected.

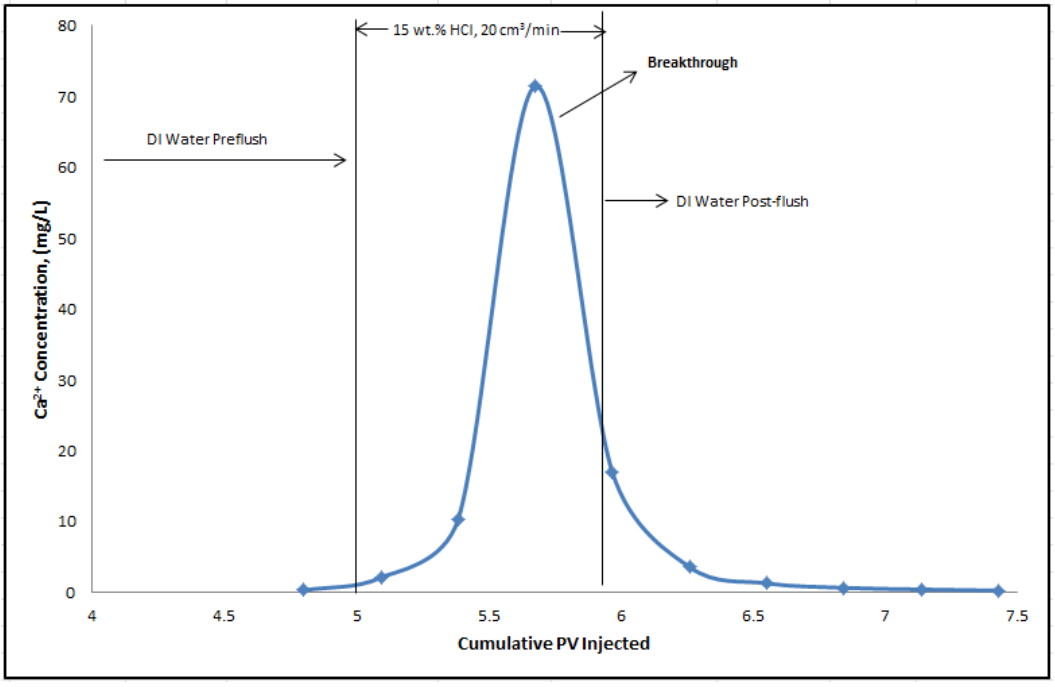

Figure IV.36: Calcium ion concentration in acid injection effluent for Experiment 9

Calcium ion concentration in the effluent starts increasing after the switch to acid injection. The concentration rises then reaches a maximum of 70 mg/L during acid injection. Calcium ion concentration decreases sharply to 3.5 mg/L after the switch to DI water injection, then gradually to zero.

REPEATABILITY

The three experiments that were performed at 1850 psi backpressure detailed in this chapter are Experiments 5, 7, and 8. These experiments were repeated at the exact same experimental conditions to test for repeatability, in terms of agreement of both PVBT results and behavior. The results of the repeated experiments are presented in Table 4.7.

Table IV.7: Results of Repeated Experiments

Experiment Number	Core Name	Acid Injection Flowrate (cm^3/min)	Backpressure (psi)	PVBT
5 (repeated)	B3-9	5	1850	0.56
8 (repeated)	B3-8	10	1850	1.16
7 (repeated)	B3-7	20	1850	0.88

CHAPTER V

INVESTIGATING THE EFFECTS OF SUPERCRITICAL CO_2 INJECTION ON BRINE SATURATED INDIANA LIMESTONE CORES

Chapter V is also divided into two parts. In the first part, titled "Experimental Plan", the laboratory tests performed to evaluate the effects of supercritical CO_2 injection on brine saturated Indiana limestone cores are outlined. The experimental procedure that is employed in these tests is also described. In the second part, titled "Results and Discussion", the results of each experiment are presented and the immediate significance of the findings is discussed.

EXPERIMENTAL PLAN

The following experiments, listed in Table 5.1, were performed to study porosity evolution and changes in pore structure resulting from injection of supercritical CO_2 into 20 inch Indiana Limestone cores saturated with NaCl solutions of different concentrations. The changes in porosity (either pore enlargement or deposition) were studied by observing changes in permeability. All experiments were performed at a supercritical CO_2 injection flowrate of 1.2 $cm^{3/}$min and a temperature of 150 °F. For all the experiments described in Chapter V, the backpressure was maintained at 1300 psi and the overburden pressure at 2000 psi.

Table V.1: Experimental Outline for Chapter V

Experiment Number	Core Name	Brine (NaCl) Solution concentration (wt.%)
10	B2-4	6
11	B2-5	12

Before the experiments could be performed, CO_2 had to be compressed in an accumulator. Also, the brine solution to be used had to be prepared. The procedures for compressing the CO_2 and preparing the brine solutions are described in Chapter II, in the section titled "Experimental Methods". The procedure for preparing the actual core samples for CO_2 flooding (saturation, porosity/pore volume and permeability determination) is also outlined in the same section, under the title of "Core Sample Preparation".

When the cores were ready to be flooded, the CO_2 compressed, and the brine solution prepared, the first step was to inject supercritical CO_2 into the DI water saturated 20 inch Indiana limestone core samples.

RESULTS AND DISCUSSION

The results for Experiment 10 are displayed in Table 5.2.

Experiment 10: 20 inch Indiana limestone core saturated with 6 wt.% NaCl solution

Table V.2: Summary of Results for Experiment 10

Core Name	B2-4
Pre-flooding Porosity (%)	15.61
Pre-flooding Pore Volume (cm3)	90.4
Pre-flooding Permeability (md)	138.2
Post-flooding Porosity (%)	15.83
Dissolved Matrix (g)	1.31

Unlike Chapter III and IV, Chapter V does not contain photographs of the core sample inlet and outlet before and after the experiment. This is due to the benign nature of CO_2 flooding in terms of matrix dissolution. The flooding procedure did not produce any noticeable differences in the inlet or outlet faces of the core samples.

The first step was to inject two pore volumes of supercritical CO_2, pressurized to 1400 psi, into the DI water saturated core sample at a flowrate of 1.2 cm^3/min. The pressure drop across the core sample during that process is displayed in Figure 5.1.

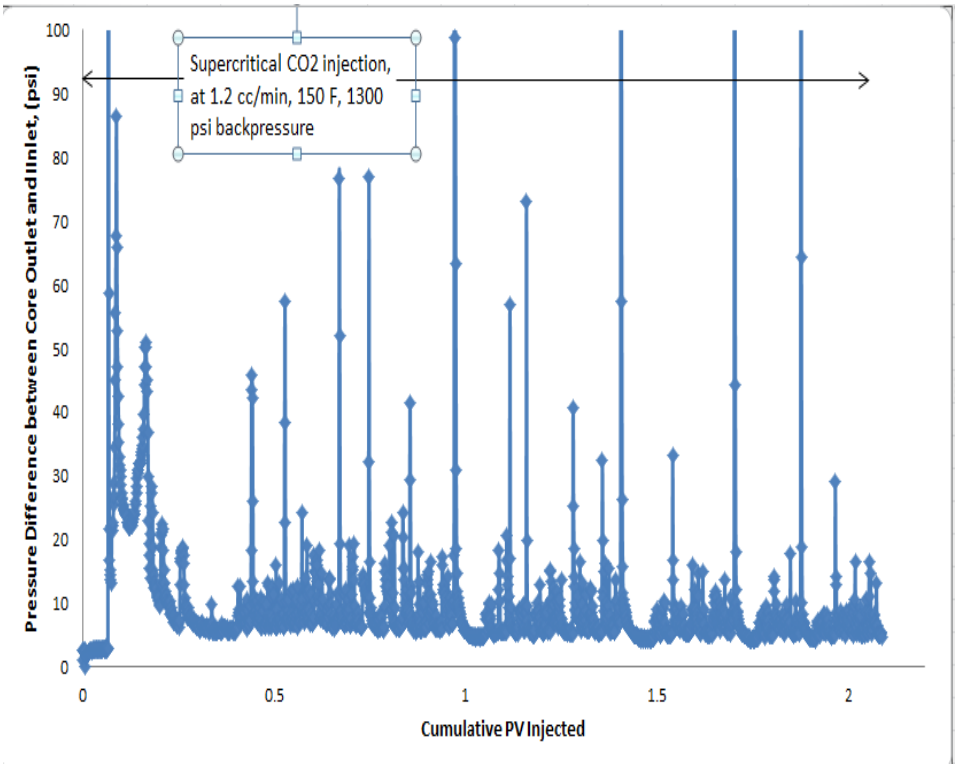

Figure V.1: Pressure drop across core sample during first injection phase for Experiment 10

This figure displays the pressure drop across the DI water saturated core as supercritical CO_2 is injected. As can be observed from the plot, the main trend in pressure drop stays constant throughout the injection. The spikes (sudden increase in pressure drop) are due to the sudden expansion of gas and it being trapped in the effluent tube then suddenly escaping in batches.

After two pore volumes of supercritical CO_2 were injected, 6 wt.% NaCl solution was injected immediately afterwards to measure the permeability of the core. The permeability of the core to 6 wt.% NaCl solution immediately after the first flooding procedure was 68 md. The core sample was then saturated with 6 wt.% NaCl solution in a vacuum chamber. The permeability of the core sample to 6 wt.% NaCl solution after

vacuum saturation with the same solution was the measured to be 81.9 md. The core was now ready to be flooded with supercritical CO_2 for the second time. The conditions for preparing and pressurizing the CO_2 in addition to its flowrate were kept constant. 2.7 pore volumes of supercritical CO_2 were injected into the 6 wt.% brine saturated core sample at 1.2 cm^3/min. . The pressure drop across the core sample is shown in Figure 5.2.

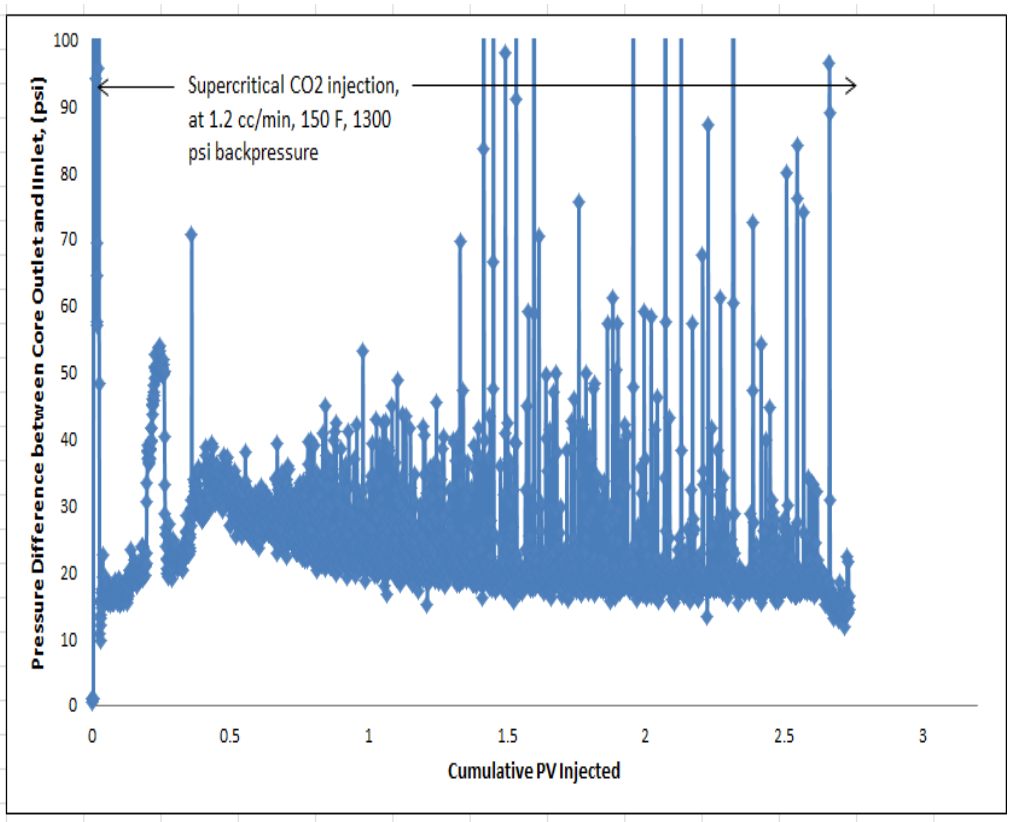

Figure V.2: Pressure drop across core sample during second injection phase for Experiment 10

The figure displayed above shows the pressure drop across the 6 wt% NaCl saturated core as supercritical CO_2 is injected into that core. Unlike the injection into the

DI water saturated core, there is a gradual decrease in pressure drop as the injection proceeds. The spikes are due to the sudden expansion of gas and it being trapped in the effluent tube then suddenly escaping in batches.

After the core was flooded a second time, its final permeability to 6 wt.% NaCl solution was measured and determined to be 75.1 md. Calcium ion concentration in the effluent samples was measured using ICP for both CO_2 injection procedures. There was no detectable level of calcium ions in the effluent samples obtained from the injection of supercritical CO_2 into DI water saturated cores. This supports the conclusion from the pressure drop plot; that supercritical CO_2 injection into the DI water saturated core caused less dissolution than injection into NaCl solution saturated cores. Calcium ion concentration for the effluent from supercritical CO_2 injection into 6 wt% NaCl saturated core is displayed in Figure 5.3.

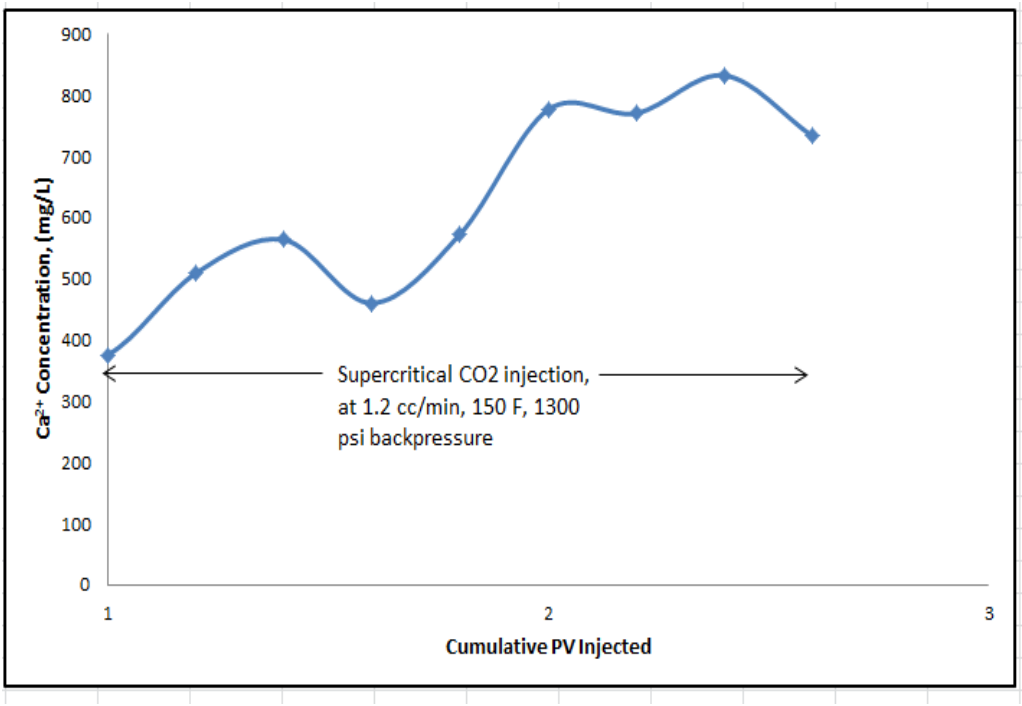

Figure V.3: Calcium ion concentration in effluent during second injection phase for Experiment 10

Calcium ion levels are too low to detect when the supercritical CO_2 injection is started. Their levels then rise steadily as the injection process proceeds and reach a maximum of 832.7 mg/L. At the end of the injection, calcium ion levels are at 733 mg/L. The core was then CT scanned after the flooding process was completed and the final permeability measured. Figure 5.4 displays the CT scan of the core sample that was employed in this experiment:

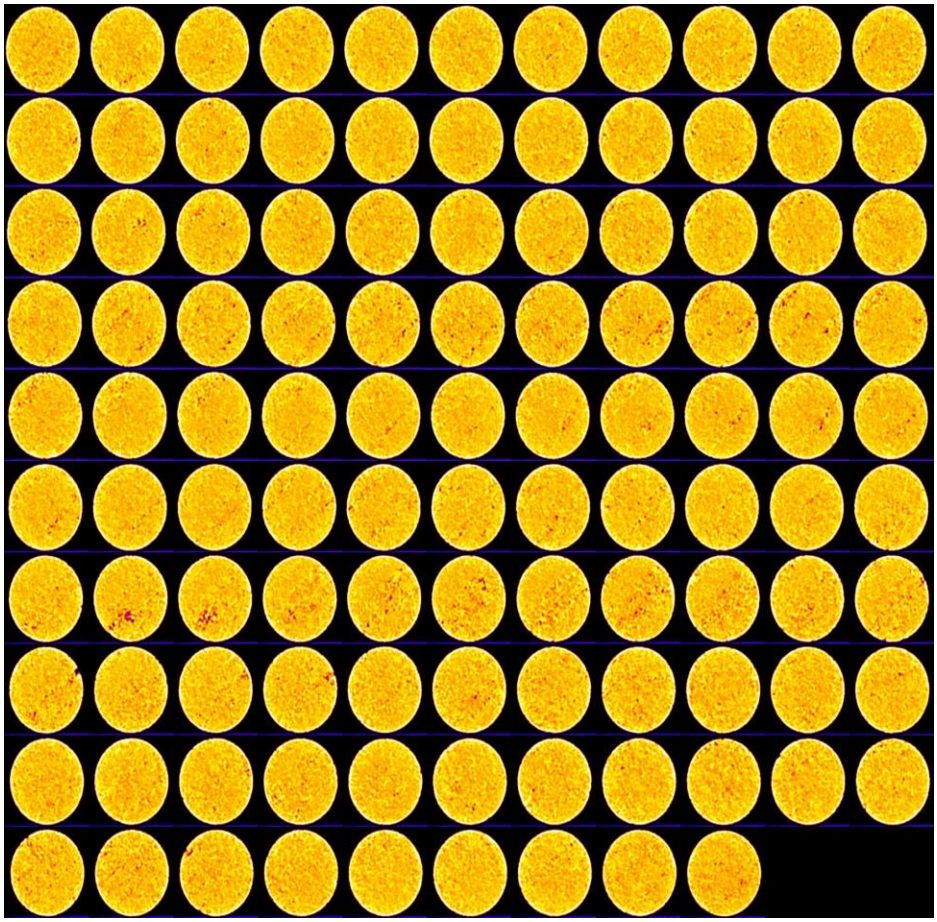

Figure V.4: CAT scan of core sample after Experiment 10

As can be seen from the figure displayed above, the CO2 injection process did not cause any major, detectable dissolution the core sample. This is inferred from the absence from strong, dark colored streaks in the figure above. There are some red patches interspersed around the center of the core, as characteristic of the vuginess typically found in high-permeability Indiana limestone samples. The results of Experiment 11 are listed in Table 5.3.

Experiment 11: 20 inch Indiana limestone core saturated with 12 wt.% NaCl solution

Table V.3: Summary of Results for Experiment 11

Core Name	B2-5
Pre-flooding Porosity (%)	16.02
Pre-flooding Pore Volume (cm3)	92.77
Pre-flooding Permeability (md)	70.4
Post-flooding Porosity (%)	16.47
Dissolved Matrix (g)	2.6

The first step was to inject 2.4 pore volumes of supercritical CO_2, pressurized to 1400 psi, into the DI water saturated core sample at a flowrate of 1.2 cm^3/min. The pressure drop across the core sample during that process is displayed in Figure 5.5.

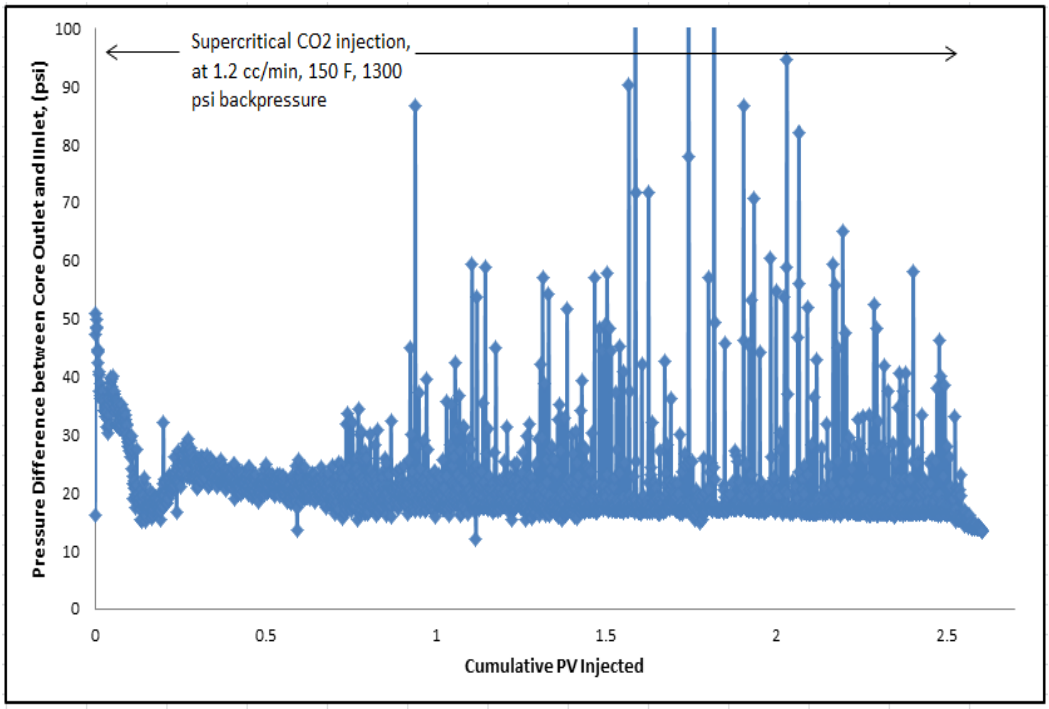

Figure V.5: Pressure drop across core sample during first injection phase for Experiment 11

This figure displays the pressure drop across the DI water saturated core as supercritical CO_2 is injected. As can be observed from the plot, the main trend in pressure drop stays constant throughout the injection. As mentioned in the previous experiment, the spikes (sudden increase in pressure drop) are due to the sudden expansion of gas and it being trapped in the effluent tube then suddenly escaping in batches.

After two pore volumes of supercritical CO_2 were injected, 12 wt.% NaCl solution was injected immediately afterwards to measure the permeability of the core. The permeability of the core to 12 wt.% NaCl solution immediately after the first flooding procedure was determined to be 60 md. The core sample was then saturated with 12 wt.% NaCl solution in a vacuum chamber.

The permeability of the core sample to 12 wt.% NaCl solution after vacuum saturation with the same solution was the measured to be 59 md. The core was now ready to be flooded with supercritical CO_2 for the second time. The conditions for preparing and pressurizing the CO_2 in addition to its flowrate were kept constant. 2.8 pore volumes of supercritical CO_2 were injected into the 6 wt.% brine saturated core sample at 1.2 cm^3/min. . The pressure drop across the core is shown in Figure 5.6.

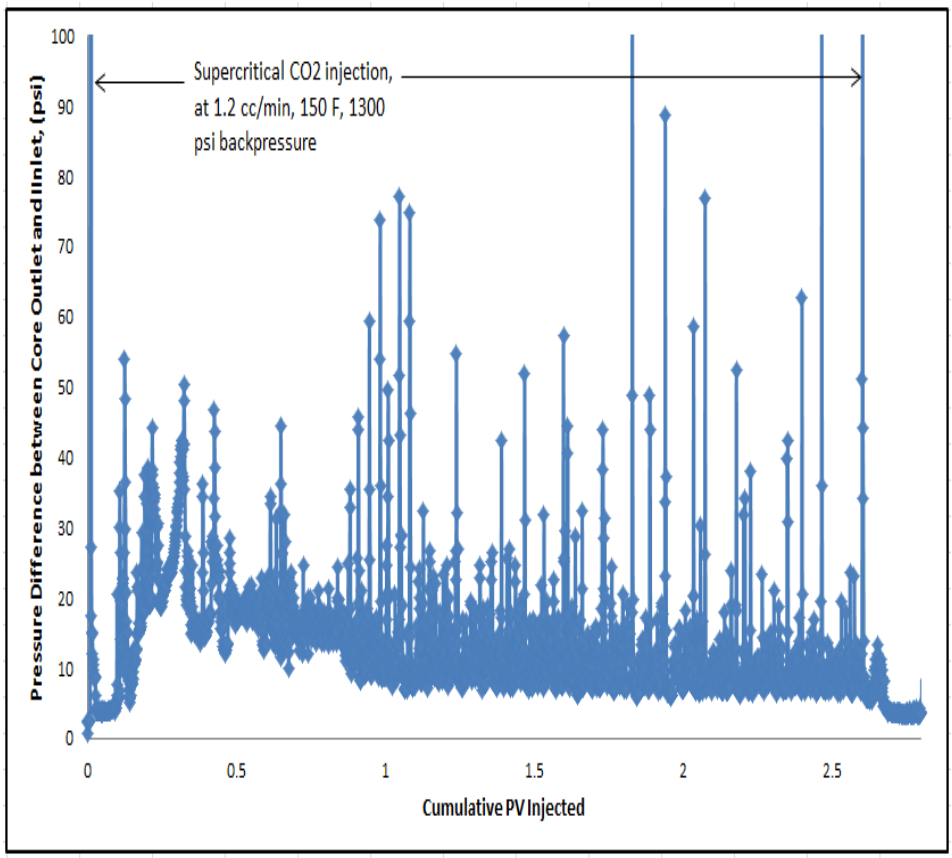

Figure V.6: Pressure drop across core sample during second injection phase for Experiment 11

The figure displayed above shows the pressure drop across the 6 wt% NaCl saturated core as supercritical CO_2 is injected into that core. Unlike the injection into the

DI water saturated core, there is a gradual decrease in pressure drop as the injection proceeds. After two pore volumes were injected, the trend appears to be mostly constant. The spikes are due to the sudden expansion of gas and it being trapped in the effluent tube then suddenly escaping in batches, as mentioned previously.

After the core was flooded a second time, its final permeability to 12 wt.% NaCl solution was measured and determined to be 46 md. Calcium ion concentration in the effluent samples was measured using ICP for both CO_2 injection procedures. The concentration of calcium ions in the effluent obtained from the injection into the DI water saturated core is displayed in Figure 5.7.

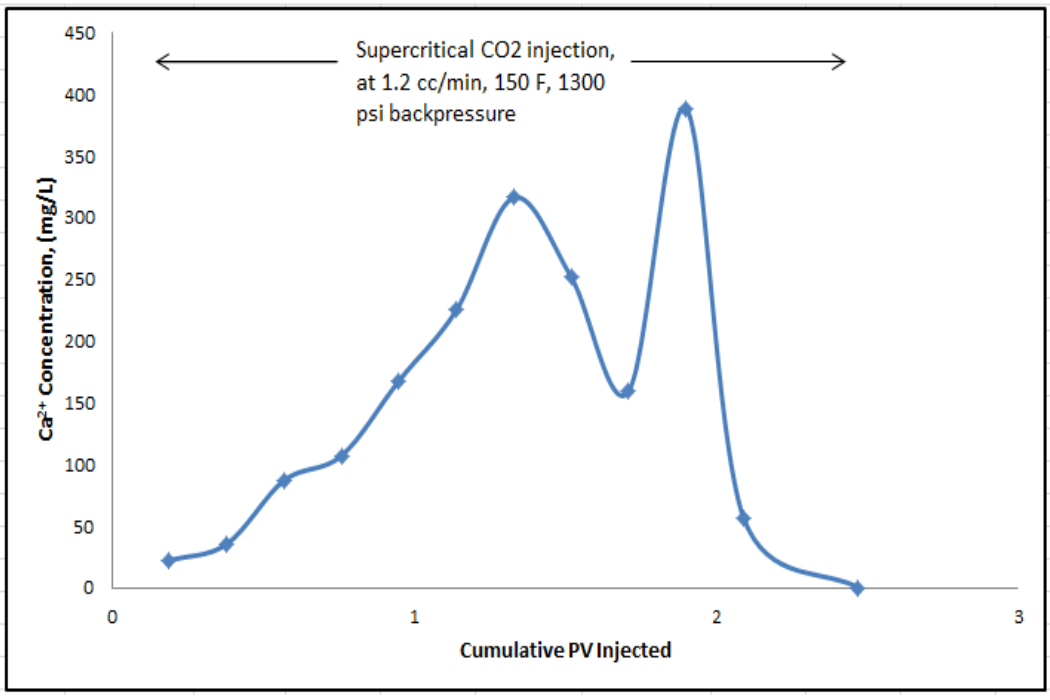

Figure V.7: Calcium ion concentration in effluent during first injection phase for Experiment 11

Calcium ion levels are initially low (less than 50 ppm) when supercritical CO_2 injection is started. The concentration then rises steadily as the injection proceeds and is the highest between the injection of the first to the second pore volume, where it reaches a maximum of 388 mg/L.

After the 2 pore volumes have been injected, the calcium ion concentration falls to zero until the end of the injection. Calcium ion concentration for the effluent from supercritical CO_2 injection into 12 wt% NaCl saturated core is displayed in Figure 5.8.

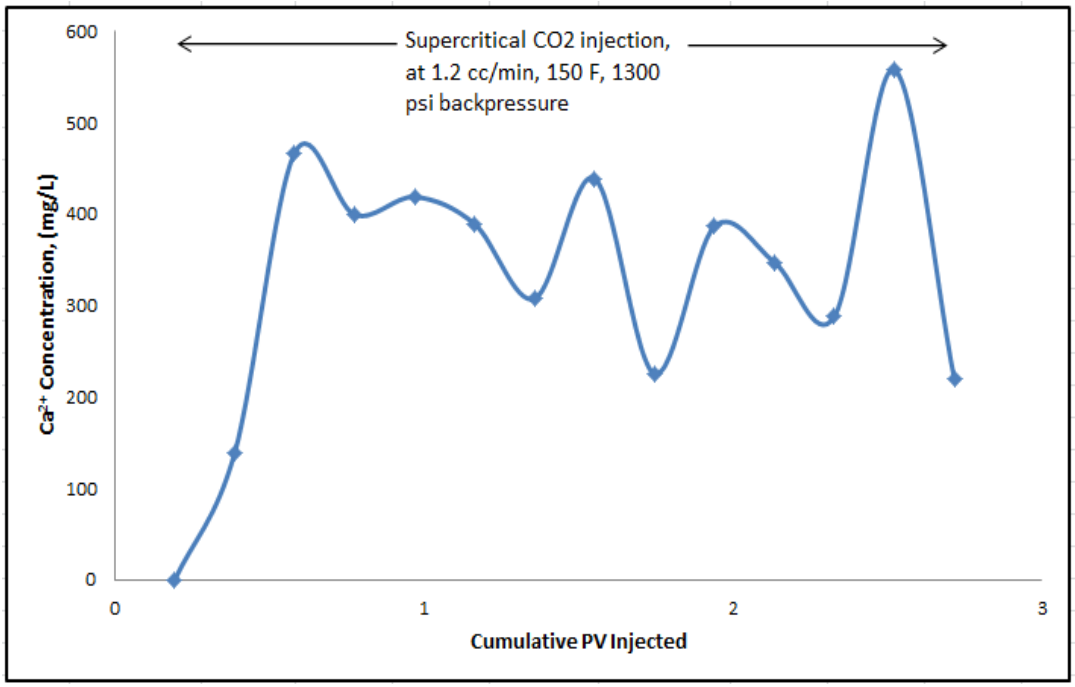

Figure V.8: Calcium ion concentration in effluent during second injection phase for Experiment 11

Calcium ion concentration rises from zero to 466.9 mg/L after the injection of 0.6 pore volumes of supercritical CO_2. The concentration then continues to fluctuate

between 466.9 and 219 mg/L for the remainder of the injection process. The maximum concentration of 558 mg/L is reached after 2.5 pore volumes are injected.

As evident from comparing the two plots of calcium concentration, we can conclude that the injection of supercritical CO_2 into the 12 wt% NaCl saturated core caused higher, more sustained levels of calcium ion concentration. This indicates that injection into the NaCl saturated core caused more dissolution in the pores when compared to the DI water saturated cores.

Figure 5.9 displays the CT scan of the core sample that was employed in this experiment.

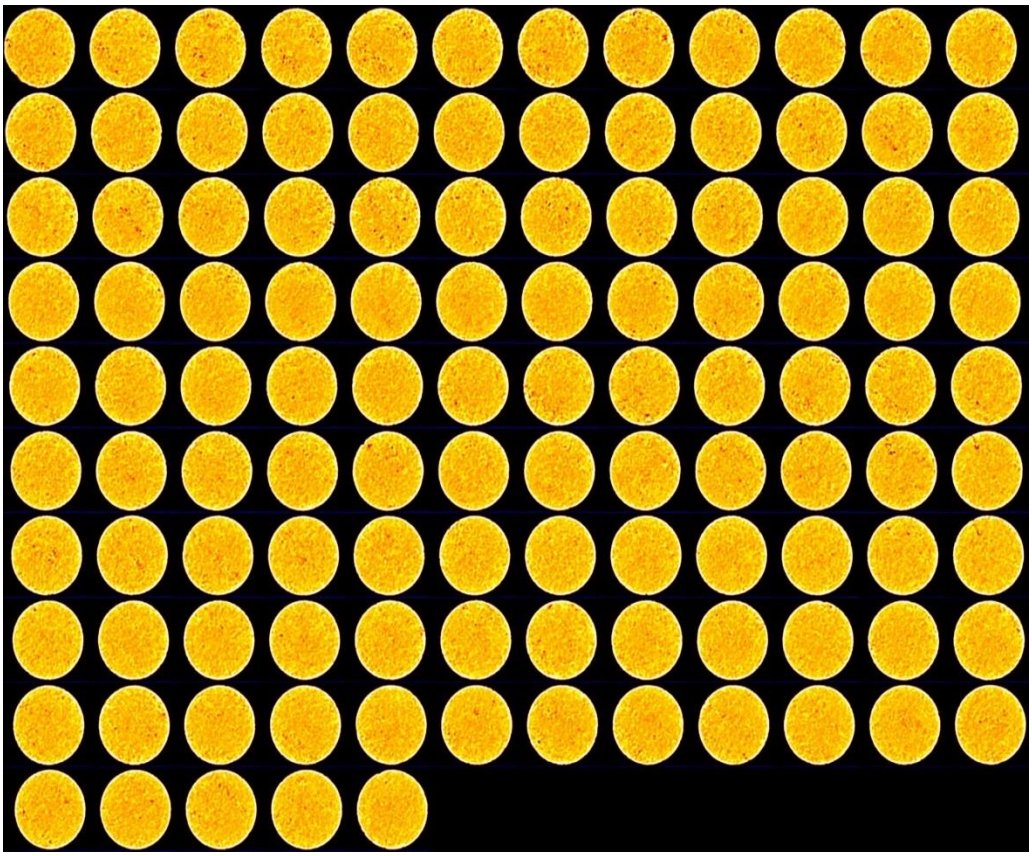

Figure V.9: CAT scan of core sample after Experiment 11

As can be seen from the figure displayed on the previous page, the CO_2 injection process did not cause any major, detectable dissolution the core sample. This is inferred from the absence from strong, dark colored streaks in the figure above. No major vuginess is observed in this core sample.

CHAPTER VI

CONCLUSIONS AND RECOMMENDATIONS

In Chapter VI, the main results from the previous chapters are summarized so as to easily compare them. The significance of the results and their implications are discussed. The experimental results and the inferences drawn from them are then used to develop recommendations that could help in performing similar tests or for future research.

Chapter III presented the results of the experiments performed to evaluate the effects of core length on PVBT behavior in 20 inch Indiana limestone cores. To that extent, the flowrate and temperature of acid injection were kept constant, and the variables were the acid concentration and the length of the core. Table 6.1 summarizes the main results of Chapter III.

Table VI.1: Major Results from Chapter III

Experiment Number	Core Name	Core Length (inch)	Acid Concentration (wt.%)	PVBT
1	B1-1	6	5	1.2
2	B1-5	20	5	6.53
3	B1-6	20	15	1.12
4	B1-9	20	5	5.26

As can be observed from the table above, increasing the length of the core leads to increased acid spending along the walls of the propagating wormhole network. This in turn translates to an increased PVBT. An important conclusion can be drawn from contrasting the images of the core inlets after acid injection for Experiment 1 when compared to Experiments 2 and 4 (please refer to chapter III for these figures). It is easily seen that there is a greater degree of face dissolution in the 20 inch cores compared to the six inch core. This is due to the fact that for 20 inch cores, 5 cm^3/min is a very low flowrate that is far below optimum for 5 wt.% HCl solution. This is confirmed by the fact that the wormhole is much larger in diameter in the inlet side of the core when compared to the outlet side of the core. This is due to the acid spending along the inlet side of the wormhole, and little live acid reaching the propagating tip of the wormhole.

This aforementioned observation is confirmed by comparing the core from Experiment 3 with the cores from Experiments 2 and 4. For 15 wt% HCl, it appears that 5 cm^3/min is closer to the optimum injection rate when compared to the 5 wt% HCl solution. For this reason, there is much less disparity in size in the diameter of the wormhole when comparing the inlet side to the outlet side. Also, there is less face dissolution observed in the inlet side of the core from Experiment 3.

Two recommendations are suggested for this part:

1) An experiment can be performed on a 6 inch core with 15 wt% HCl solution, and the PVBT can be contrasted with that from Experiment 3.
2) Experiment 2 and 4 show a 19% difference in PVBT. The experiments can be repeated to ensure validity, and confirm if the increased backpressure in Experiment 4 is the cause for the decrease in PVBT.

Chapter IV presented the results of the experiments performed to evaluate the effects of flowrate on PVBT behavior in 20 inch Indiana limestone cores. To that extent, the acid concentration and the temperature of acid injection were kept constant, and the variables were the acid flowrate and the backpressure applied on the core. Table 6.2 summarizes the main results Chapter IV.

Table VI.2: Major Results from Chapter IV

Experiment Number	Core Name	Flowrate (cm3/min)	Backpressure (psi)	PVBT
5	B3-1	5	1850	0.2
6	B3-2	10	1000	0.5
7	B3-3	20	1850	0.7
8	B3-4	10	1850	1.22
9	B3-5	20	1000	0.53

By contrasting Experiment 3 from Chapter III (B1-6) with Experiment 5 from Chapter IV (B3-1), it is observed that there is a great drop in the PVBT value. This is unexpected as the conditions for both experiments are identical, with the exception of the increased backpressure for core B3-1. This could either be due to experimental factors such as the internal structure of the core, or due to the increased backpressure applied on the core.

The increased backpressure acts to keep CO_2 in solution, where at 1000 psi some CO_2 is present is a subcritical state, which could form gas bubbles that can impede mass transfer at the fluid-rock interface and hence increase the PVBT. This however is unconfirmed, as for Experiments 6 and 8 tabulated above, the PVBT increases as the backpressure increases. The experiments performed at 20 cm^3/min (Experiments 7 and 9) follow the same trend and show an increase in PVBT with increasing backpressure.

It is worth noting that the experiments performed at 5 and 20 cm^3/min show more ramifications and branching in the dissolution behavior when compared to Experiment 6, performed at 10 cm^3/min. It is also interesting that the wormhole observed at the outside surface of the core sample for Experiment 7 travels at a straight line, and does not show as much convolution as the other experiments. The main recommendation based on the experimental work in this chapter is to perform more experiments at multiple flowrates, so as to investigate the optimum injection rate in 20 inch cores, and contrast it with that of 6 inch cores of the same lithology at the same acid concentration.

Chapter V presented the results of the experiments performed to evaluate the effects of supercritical CO_2 injection on 20 inch brine-saturated Indiana limestone cores. To that extent, the CO_2 injection flowrate and the temperature of injection were kept constant, and the only variable was the weight concentration of the brine (NaCl) solution. Table 6.3 summarizes the main results of Chapter V.

Table VI.3: Major Results from Chapter V

Experiment Number	Core Name	Brine Conc.	Initial Permeability (md)	Permeability 1 (md)	Permeability 2 (md)	Permeability 3 (md)
10	B2-4	6	138.2	68	81.9	75.1
11	B2-5	12	70.4	60	59	46

Where,

Permeability 1: Permeability to brine immediately after CO_2 injection into DI water saturated core sample

Permeability 2: Permeability to brine after vacuum saturation with brine solution of the same concentration

Permeability 3: Permeability to brine after CO_2 injection into brine saturated core sample

Based on the results summarized in the table above, we conclude that supercritical CO_2 injection into Indiana limestone cores causes formation damage and subsequently a lower final permeability. This is in agreement with findings displayed in the literature. The damage mechanism is due to the nature of the chemical equilibrium that exists in this system. Initially, the CO_2 injection produces carbonic acid as the gas dissolves in water. This acid causes the formation of the soluble bicarbonate species:

$$CaCO_3 + H_2O + CO_2 \rightleftharpoons Ca(HCO_3)_2$$

This leads to an enhancement in permeability in the initial section of core. However as the injection continues, and the pH rises as the fluid travels along the core due to spending, and the propagating carbonic acid keeps producing more bicarbonate, the equilibrium starts shifting to the left. This leads to the deposition of calcium carbonate, which causes formation and leads to an overall reduced permeability in the core sample.

Another important recommendation can be drawn by observing and comparing the calcium ion concentration plots from the 6 wt.% and 12 wt.% brine experiments. Even though the solubility of CO_2 is lower in 12 wt.% brine than it is in 6 wt.%, more

calcium ions are liberated in the second experiment. This anomaly is consistent with the literature, and is an interesting area of possible research.

REFERENCES

Bazin, B., Roque, C. and Bouteca, M. 1995. A Laboratory Evaluation of Acid Propagation in Relation to Acid Fracturing: Results and Interpretation. Paper SPE 30085 presented at the European Formation Damage Conference, The Hague, Netherlands, 15-16 May. DOI: 10.2118/30085-MS.

Buijse, M., de Boe, P., Breukel, B., and Burgos, G. 2004. Organic Acids in Carbonate Acidizing. *SPE Prod & Fac* **19**(3): 128-134.

Daccord, G. 1987. Chemical dissolution of a porous medium by a reactive fluid. *Phys. Rev. Lett.*, 58, 479.

Daccord, G., Leonormand, R. and Lietard, O. 1993a. Chemical Dissolution of a Porous Medium By A Reactive fluid-1. model for the "Wormholing" Phenomenon. *Chem. Eng. Sci.*, 48, 169.

Daccord, G., Leonormand, R. and Lietard, O. 1993b. Chemical Dissolution of a Porous Medium By A Reactive Fluid-2. Convection vs Reaction, Behavior Diagram. *Chem. Eng. Sci.*, 48, 179.

Daccord, G., Touboul, E. and Lenormand, R. 1989. Carbonate acidizing: Toward a Quantitative Model of the Wormholing Phenomenon. *SPE Production Engineering*, Feb. 1989, 63.

Fredd, C.N. and Fogler, H.S. 1998. Alternative Stimulation Fluids and Their Impact on Carbonate Acidizing. *SPE J.* **3**(1): 34-41.

Fredd, C.N. and Fogler, H.S. 1999. Optimum Conditions for Wormhole Formation in Carbonate Porous Media: Influence of Transport and Reaction. SPE Journal, **4**(3): 196-205. SPE-56995-PA. doi:10.2118/56995-PA.

Frick, T.P., Mostofizadeh, B., and Economides, M.J. 1994. Analysis of Radial Core Experiments for Hydrochloric Acid Interaction with Limestone. Paper SPE 27402 presented at the SPE International Symposium on Formation Damage Control, Lafayette, Luisiana, 7-10 February. doi: 10.2118/27402-MS.

Hill, A.D. Zhu, D., and Wang, Y. 1995. The Effect of Wormholing on the Fluid-Loss Coefficient in Acid Fracturing. SPE Prod & Fac **10**(4): 257-26224. SPE-27403-PA. doi: 10.2118/27403-PA.

Hoefner, M.L. and Fogler, H.S. 1987. Role of Acid Diffusion in Matrix Acidizing of Carbonates. *SPE Journal of Petroleum Technology* **39** (2): 203-208. doi: 10.2118/13564-pa

Hoefner, M.L. and Fogler, H.S. 1988. Pore Evolution and Channel Formation During Flow and Reaction in Porous Media. *AIChE Journal* **34** (1): 45-54. doi: 10.1002/aic.690340107

Hoefner, M.L. and Fogler, H.S. 1989. Fluid-Velocity and Reaction-Rate Effects During Carbonate Acidizing: Application of Network Model. *SPE Production Engineering* **4** (1): 56-62. doi; 10.2118/15573-PA

Huang, T., Hill, A.D., and Schechter, R.S. 1997. Reaction Rate and Fluid Loss: The Keys to Wormhole Initiation and Propagation in Carbonate Acidizing. Paper SPE

37312 presented at the International Symposium on Oilfield Chemistry, Houston, 18-21 February. Doi: 10.2118/37312-MS.

Nierode, D.E. and Williams, B.B. 1971. Characteristics of Acid Reaction in Limestone Formations. *SPE J*. **11**(4): 406-418.

Robert, J.A., and Crowe, C.W. 2000. Carbonate Acidizing Design. Reservoir Stimulation, 3rd Ed. Wiley, New York. p. 17.

Schechter, R.S. and Gidley, J.L. 1969. The Change in Pore Size Distribution from Surface Reactions in Porous Media. *AIChE Journal* **15** (3): 339-350. doi: 10.1002/aic.690150309

Talbot, M.S. and Gdanski, R.D. 2008. Beyond the Damköhler Nuber: A New Interpretation of Carbonate Wormholing. Paper SPE 113042 presented at the SPE Europec/EAGE Annual Conference and Exhibition, 9-12 June. 10.2118/113042-MS.

Wang, Y., Hill, A.D., and Schechter, R.S. 1993. The Optimum Injection Rate for Matrix Acidizing of Carbonate Formations. Paper SPE 26578 presented at the SPE Annul Technical Conference and Exhibition, Houston, Texas, 3-6 October. doi: 10.2118/26578-MS.

Williams, B., Gidley, J., and Schechter, R.S. 1979. Acidizing Fundamentals, Richardson: SPE Monograph Series.